

Atomistic Simulation Methods and their Application on Fracture

Bernhard Eidel ^{*}, Alexander Hartmaier ^{*} and Peter Gumbsch [†]

^{*} Interdisciplinary Centre for Advanced Materials Simulation (ICAMS),
Ruhr-Universität Bochum, Stiepeler Strasse 129, 44801 Bochum, Germany

[†] Institut für Zuverlässigkeit von Bauteilen und Systemen, Universität Karlsruhe
and Fraunhofer Institut für Werkstoffmechanik, Wöhlerstr. 11, 79108 Freiburg,
Germany

Abstract *The present work on the molecular dynamics method covers the theoretical background of the method and gives practical examples to demonstrate its capabilities and limitations. The work focusses on topics which reveal fundamental mechanisms associated with fracture processes. Moreover, promising hybrid methods based on a concurrent atomistic/continuum coupling are reviewed since they combine accuracy and efficiency in a most favorable manner.*

1 Introduction

For many engineering questions connected to the mechanical properties of materials, one can of course profitably apply continuum mechanical descriptions of materials behaviour. However, when it comes to describing small specimens or when material specific questions need to be addressed, it is usually indispensable to investigate defect properties. For plastic deformation, discrete dislocation simulations (see (Kubin et al., 1992; Devincere and Roberts, 1996; Deshpande et al., 2003; Weygand et al., 2002; Weygand and Gumbsch, 2005) or the article by V. Mohles in this collection) can be applied. In these simulations the interaction of dislocation with interfaces determines the influence of the microstructures. These discrete defect based methods, however, require governing laws for the individual defect properties and more detailed descriptions for the short range interaction of defects. Such properties are difficult to obtain experimentally and are therefore usually investigated by atomistic methods.

Therefore, atomistic modelling is essential in advancing our understanding of the mechanical properties of materials. This is most obvious for the investigation of fracture processes. Materials behaviour with respect to fracture is of course ultimately determined by events on the atomic scale.

In the case of brittle fracture this connection is obvious, since the crack in a perfectly brittle material must be atomically sharp at its tip. The crack moves by breaking individual bonds between atoms and can therefore be regarded as a macroscopic probe for the atomic bonding. The transition from perfectly brittle to ductile behaviour similarly relies on atomistic processes since the multiplication or nucleation of dislocations at the crack tip is an indispensable ingredient of any modelling of the brittle to ductile transition. Atomistically the nucleation or multiplication of dislocations at the crack tip is identified with bond shearing events, which compete with the bond breaking events at crack extension.

The interaction of multiple defects, like cracks and dislocations, is still not routinely studied even with the simplest atomistic simulation methods since such studies necessarily require models that significantly extend in all three dimensions and consequently require the handling of millions of atoms. Since the application of atomistic techniques has great potential (Li et al., 2003; Kassner et al., 2005) but is still not widespread in the investigation of the mechanical properties of materials, it is probably advisable to give a short overview on the applicable methods and then to provide a few examples of successful application of atomistic modelling techniques to explain experimentally observed phenomena.

In the following section we give a general overview of the different descriptions for the atomic bonding, because they are the basis for all atomistic modelling. The next section describes the molecular dynamics method in some detail, also including the boundary conditions and visualisation of defects. This part is intended to give the reader, who is not familiar with atomistic simulation methods a feeling for the versatility of this approach. The capabilities and limitations of atomistic methods are not just related to the available description of the atomic bonding but also to the handling of boundary conditions and the analysis of the results. The subsequent section 4 deals with concurrent multiscale methods, which couple atomistic and continuum descriptions in a rather seamless manner, hence enabling the description of crystalline solids with atomistic accuracy but at smaller computational costs. The Finite Element Atomistic Method (FEAt) and variants of the Quasicontinuum (QC) method are reviewed and compared.

After this methods-oriented part, in Section 5 the phenomenology of fracture is discussed in the light of atomistic modelling. First, brittle fracture is put in the spotlight, which is the domain of the atomistic methods, as we have seen above. Second, it is shown that the analysis of the plastic zone around a crack tip is now within the scope of large scale atomistic simulations.

It is noted here that this article can neither provide a practical guide

for the use of atomistic methods nor can it claim to give an exhaustive overview of all the work where these methods provide insight into atomistic processes of fracture. It is rather meant to be a first introduction into the topic, highlighting a few illustrative examples and showing the possibilities and limitations of the most frequently used methods. Interested readers should also consult recent overviews on the subject (Li et al., 2003; Kassner et al., 2005) for more details and for additional references.

In order to limit the references to a useful number, we restrict ourselves to citations concerning models and numerical simulations to the literature dealing with fracture, where adequate. Furthermore, if the same authors published a number of articles on similar topics in fracture, the most recent work is usually given here since it will often provide guidance to previous work.

2 Description of Interatomic Bonds

In this section the different atomistic methods that have been used to model fracture processes are briefly introduced. The scope of this section is to give a general introduction into the basic idea behind the atomistic, *i.e.* non-continuum, method being used to model fracture of materials, to introduce the essential terms, and to provide the basic literature for further reading. No attempt is made to provide cooking recipes enabling the reader to implement such methods solely based on this text.

Before presenting the different methods to describe the atomic interaction, it is worth mentioning that atomistic modelling may be applied with very different intentions. In some cases, the atomistic simulations are used as testing grounds for ideas about the behaviour or energetics of defects. It may then be perfectly justified to use the simplest generic form of the interaction model. Alternatively, the goal may be to make quantitative or semiquantitative predictions about the properties of specific materials. In this case one has to resort to materials-specific models or even quantum mechanical *ab initio* methods.

2.1 Quantum Mechanics Based Descriptions of the Atomic Bonding

The most fundamental description of interatomic bonds that may have ionic, covalent, metallic or van-der-Waals character, or any mixture of these pure bond types, is given by explicitly dealing with all the electrons involved in the formation of the atomic bonds. The quantum mechanical description of a crystalline material is a classical problem of solid state physics and

appropriate tools have been developed there, which today are available for the use in many different application areas. In all these codes, the many-body problem of atomic nuclei and electrons must be solved for different geometries. Lattice periodicity is usually imposed. The solution is generally approached in three steps:

1. Within the Born-Oppenheimer approximation the motion of the atomic nuclei is (adiabatically) decoupled from the motion of the electrons. Since the mass and the inertia of the atomic nuclei is orders of magnitude larger than the mass of the electrons, the electronic quantum gas follows the motion of the nuclei almost instantaneously. Furthermore the electrons are always assumed to remain in their ground state with respect to the momentary position of the nuclei.
2. The quantum mechanical ground state of the inhomogeneous electron system in the system of the nuclei is determined then in an external electrostatic potential, given by the charge at the instantaneous position of the nuclei. In practical calculations, the many particle state of the interacting electrons is usually constructed from single particle states of non-interacting electrons in an effective (mean) field of all the other electrons. These single particle states are self consistently determined by iteratively solving the coupled set of single particle problems for all the electrons. The most successful approach to this problem has been *density functional theory (DFT)* (Hohenberg and Kohn, 1964; Kohn and Sham, 1965). Within the *local density approximation (LDA)* it is assumed that the exchange correlation of the electrons can be calculated based purely on the local electron density. This is sometimes not enough and generalised gradient approximations (GGA) have been introduced.
3. In the last step we now reintroduce the motion of the atomic nuclei. The ground state energy of the electron gas can be regarded as the potential energy for the nuclei in their configurational space. The atomic motion can then be simulated in this *adiabatic* potential. Local minima in this adiabatic potential reflect statically stable structures for the solid while saddle points are the static barriers for structural transformations. With the knowledge of the adiabatic potential, it is possible to determine kinetic, dynamic or statistical materials properties (e.g. phonon properties, transport properties, or phase equilibria) either by classically solving Newtons equations of motion, by minimising the total energy of a structure or by solving quantum mechanical problems for the nuclei (e.g. for zero point vibrations of light elements).

The main task of electron theory is to solve for the electronic ground state, the second step above, in a numerical way. There are several successful methods available to do so, based on plane waves, localised orbitals or a mixture of them. The Cambridge (Serial) Total Energy Package CASTEP, the Vienna Ab-initio Simulation Package VASP or the Mixed Basis Pseudo-Potential Code MBPP are standard packages for this task.

Since these quantum mechanical methods do not require any adjustable parameters and are therefore often termed *ab initio* or *first principles* techniques. Their results provide highly accurate and predictive results on materials properties.

However, the methods are computationally very demanding and often require periodic structures, which are constructed by defining a unit cell comprising the atoms to be considered and repeating this unit cell periodically in all directions. This procedure is identical to the periodic boundary conditions that are used extensively in molecular dynamics simulations, as will be described below. However, the periodic cells in molecular dynamics simulations may contain several million atoms, while *ab initio* methods, due to their mathematical complexity are restricted to hundreds of atoms within the unit cells. This limitation is rather severe for applications in mechanical problems, because the generation of defects or the driving force on a defect, like the energy release rate during crack advance, all depend on the total elastic energy stored within the volume. Hence, if the volume under consideration is extremely small, the elastic strains in the volume have to be close to their theoretical limits in order to store sufficient elastic energy to drive the defects. Therefore, *ab initio* simulations of defect behaviour must always be carefully checked for size effects and artifacts caused by the restrictions on the effective volume. Notwithstanding these words of warning, it must be stated again that *ab initio* methods are the most fundamental methods available to describe behaviour of materials and thus possess the most predictive power. There are also some interesting and potentially fruitful ideas to combine *ab initio* methods with molecular dynamics simulations which will be described in section 4.6.

Before leaving this section it is worth mentioning that *ab initio* methods are not just applied to study some specific fracture problem, they also play an important role in the verification and the adjustment of simpler models of the atomic interaction. To develop material-specific (semi-) empirical interaction models, various adjustable parameters and sometimes even the functional form of the interaction model has to be chosen to reproduce available data. However, experiment will usually only provide data close to mechanical and thermodynamic equilibrium, whereas the interaction models will be used at grain boundaries or even in the highly strained region near

crack tips. Therefore it is advisable to adjust the parameters of the interaction models so that they perform well under these circumstances. Because of the lack of experimental data, *ab initio* calculations of large deformations or structural energy differences are often used instead. It therefore turned out to be very useful to build up extensive *ab initio* data bases for the development of simpler interaction models. While the first such data bases for aluminium (Ercolessi and Adams, 1994) or the intermetallic nickelaluminide B2-NiAl (Ludwig and Gumbsch, 1995) still constituted demanding calculations, such databases can today be generated routinely and very systematically.

2.2 Atomic Interaction Models, Potentials

While it is generally possible to use *ab initio* methods to study the dynamic evolution of an atomistic system, the computational burden is usually too high and (semi-)empirical potentials are therefore applied in molecular dynamics (MD) simulations. The atomic interaction as described by semi-empirical potentials always depends on the distance of interacting pairs of atoms and, for the more elaborate potentials, also on the bond angles and the local electron density. All these distance or angle dependent functions are represented either analytically or as tabulated functions of these parameters. The most simple pair potentials, like Lennard-Jones or the Morse potential, have just two or three free parameters that are used to change the characteristic properties of the potential like the lattice parameter, the bulk elastic modulus or the cohesive energy. More sophisticated potentials have a number of free parameters that yield much better results for material specific properties like lattice constant, sublimation energy, anisotropic elastic constants, vacancy formation energy, stacking fault energy, or whatever is felt necessary for a certain investigation. The free parameters of the potentials are usually fitted to material properties by calculating exactly these properties on rather small atomic ensembles and then varying the potential parameters until a reasonable match to experimental or *ab initio* data is reached. The interatomic potentials can roughly be categorized into three classes according to their level of approximation of the "real" quantum mechanical atomic interaction:

- angularly-dependent tight-binding or bond-order potentials
- multibody or embedded atom method (EAM) potentials
- pair potentials

The properties and characteristics of the different potentials are given in some detail below. For application purposes, the choice of a potential will usually involve a trade-off between the accuracy of the description of the atomic interaction from first principles calculations over semi-empirical po-

tentials to simple pair potentials and the size of the system that can be studied, *i.e.* the number of atoms that can be explicitly treated in the sample. The decision, whether higher accuracy in the description of the interatomic forces or larger system size, has to be made for each problem under consideration. For example, during fracture of covalently bonded systems like silicon, polymers or biological matter the behaviour of the entire system depends critically on the behaviour of the individual atomic bonds immediately in front of the crack tip (see Section 5.1). Here it becomes necessary to accurately evaluate the interatomic forces in order to obtain meaningful results. In contrast, for rather generic investigations of dynamic crack stability as a function of crack driving force, where the energy release rate and the stored elastic energy in the solid are decisive, it may be essential to have a reasonably large system (Gumbsch et al., 1997; Buehler et al., 2003). Even in these cases, however, materials-specific questions must again be treated with the more accurate DFT descriptions or coupled methods (Kermode et al., 2008).

Pair potentials. Pair potentials are the simplest form of interatomic potentials. This approach limits the interaction between two atoms to a dependence on their mutual distance, thus excluding completely any information about neighbouring atoms. Pair potentials in their most general form are written as

$$U_{\text{tot}} = \frac{1}{2} \sum_{i,j \neq i} V_{ij}(r_{ij}) + U(\Omega) \quad (1)$$

where V_{ij} is the pair potential, r_{ij} is the separation between atoms i and j and $U(\Omega)$ is a contribution to the cohesive energy which depends on the average volume per atom Ω . This latter term may mainly determine the cohesive energy, while the pair potential always determines the structural dependence.

Often, however, it is not attempted to mimic the properties of a particular material but more generic atomistic questions are of interest. Then, potentials like the Lennard-Jones potential or the Morse potential are applied. These have only few adjustable parameters, which are fitted to the nearest neighbour distance and the binding energy or the bulk modulus. Despite their simplicity and the lack of materials specificity, pair potentials can contribute significantly to our understanding of material behaviour and fracture in particular. Their simple structure permits investigation of generic effects, e.g. of the atomic size or of the role of elastic properties for a certain phenomenon. Other examples are when the consequences of the discrete crystal structure of solids shall be compared to predictions of

continuum models or when the influence of non-linearities in the elastic behaviour shall be mentioned that can ideally be compared with linear-elastic solids described by a harmonic pair potential (Buehler et al., 2003). In these examples use is made of the simplicity of pair potentials that allows clean studies of single effects, while excluding all other influences that render the behaviour of "real" materials so much more complex.

Of course, pair potentials cannot be used to describe situations where directional bonds or bond angles play a role. They are also not well suited to describe metals because the well established dependence of bond strength on coordination cannot be represented. Furthermore, simple pair potentials result in extremely low stacking fault energies, because they fail to distinguish the energy difference between face centred cubic (fcc) and hexagonal close-packed (hcp) structures.

Embedded atom method (EAM) potentials. The most widely used interaction models for metals are the EAM potentials. In this scheme the volume-dependent term from Equation (1) is expressed as a local density-dependent contribution to the total potential energy

$$U_{\text{tot}} = \frac{1}{2} \sum_{i,j \neq i} V_{ij}(r_{ij}) + \sum_i F(\rho_i) \quad (2)$$

with

$$\rho_i = \sum_{j \neq i} \rho_{ij}(r_{ij}) \quad (3)$$

where ρ_{ij} can be viewed as the contribution from atom j to the total electron density at atom i and F is the embedding energy associated with placing atom i in this environment. Finally, V_{ij} is the pair potential contribution to the potential energy of atom i . Different physical interpretations of the terms are possible and consequently the functional forms and the way in which the various parameters are determined may differ. Usually the functions are adjusted to reproduce at least the lattice parameter, the cohesive energy and the anisotropic elastic constants of the metal under consideration. For alloys it is additionally necessary to adjust structural energy differences of intermetallic phases and heats of solution (Ludwig and Gumbsch, 1995). As mentioned above, it is also desirable to not only adjust to such equilibrium crystal properties, but to also compare to some *ab initio* data from atomic structures far from equilibrium or for large deformations. Reliable and well tested potentials are available for the noble metals and nickel as well as for some aluminium alloys (e.g. (Ercolessi and Adams, 1994; Ludwig and Gumbsch, 1995; Mishin et al., 2001)).

The main advantage of EAM potentials is that they can be applied to inhomogeneous systems such as surfaces or cracks, since these potentials approximately incorporate the variation of bond strength with coordination. Decreasing the coordination (density) at an atom usually increases the strength of each of its bonds and decreases the bond length. In particular for fcc materials it has been easily possible to reproduce anisotropic elastic constants, sublimation energy, vacancy formation energy, surface and stacking fault energies with EAM potentials and EAM potentials can be applied to many different types of simulations. For body centred cubic (bcc) metals the method may still give a sufficiently precise description. For some of these metals, however, it has been shown that the EAM fails to give a valid description of the core structure of dislocations (Mrovec et al., 2004) and thus the Peierls stress to move the dislocation through the lattice. Therefore, these potentials cannot be used reliably to model plasticity in these materials. This may be seen as an indication of the importance of angular bonding characteristics and one may consequently resort to tight binding or bond order descriptions (Pettifor and Oleinik, 1999; Mrovec et al., 2004, 2007a).

Tight binding and bond order potentials. The need for material specific models and for accuracy in atomistic simulations implies that a quantum mechanical description of the atomic interaction is required. The semi-empirical tight binding scheme is such an approximate quantum mechanical description of the energetics of systems of atoms (Harrison, 1980; Pettifor, 1995). The total energy of a system is given by:

$$U_{\text{tot}} = U_{\text{rep}} + U_{\text{bond}} \quad (4)$$

where U_{rep} is a repulsive energy, generally given as a sum of pair potentials and U_{bond} is the bonding part of the energy. The latter is obtained by solving the eigenvalue problem for a given Hamiltonian, which is assumed to be fixed and not evaluated self-consistently as in the *ab initio* methods.

The Hamiltonian matrix elements are usually assumed to be rapidly decaying functions of the atomic separation, which have to be empirically adjusted to experimental data or results of *ab initio* calculations to give a material-specific model. The least clear but most important question in this context is the transferability of these matrix elements from ideal structures to highly distorted atomic environments.

The semi-empirical tight-binding scheme is in principle applicable to materials with various types of bonding but is most naturally suited to covalently bonded insulators and semiconductors as well as the transition metals and intermetallics .

The key computational aspect in solving a tight-binding model is the diagonalisation of the eigenvalue problem. This can of course be attempted in reciprocal space, where a whole set of very efficient methods is available, which however usually scale to the third power with the number of atoms in the system. Linear scaling can be achieved with real space methods of which the density matrix method for semiconductors and insulators and the bond order approach for metals and alloys are the most promising approaches. In the simplest approximations the latter can even be formulated analytically within the framework of bond order potentials (Pettifor and Oleinik, 1999) where the energy of the system is written as

$$U_{\text{tot}} = \frac{1}{2} \sum_{i,j \neq i} V_{ij}(r_{ij}) + \sum_{i\alpha,j\beta} H_{i\alpha,j\beta} \Theta_{i\alpha,j\beta} \quad (5)$$

where V_{ij} is the pair potential, depending on the type of atom and r_{ij} is the separation between atoms i and j . H is the Slater Koster hopping integral, which also depends on distance r_{ij} and where the Greek indices stand for the type of orbital. Θ is the bond-order matrix which gives the difference in the number of electrons in the bonding and antibonding states. Modern bond order potentials for carbon (Mrovec et al., 2007b) and some transition metals (Mrovec et al., 2004, 2007a) are just becoming available.

In the same spirit as the bond-order potentials, several simplified angularly-dependent potentials of Tersoff and Brenner-type have been developed for silicon and the hydrocarbons (see for example (Pastewka et al., 2008)). These potentials have seen continuous improvements but were notoriously difficult to adjust to bond breaking problems. Despite recent success with an explicit screening formulation for the hydrocarbons (Pastewka et al., 2008) giving up specific bonds in a way which does not require a self-consistent formulation of the electronic configuration remains an important and difficult problem.

3 The Molecular Dynamics Method

To continue we describe the pertinent methods used in atomistic simulations with some focus on the application in fracture processes and related problems. We start out in the present section with the Molecular Dynamics (MD) method. A short overview of the main ingredients like time integration and relaxation is given, furthermore the role of boundary and initial conditions is described and illustrated for mechanical problem sets in materials science. Section 3.6 gives a brief account of the visualisation and analysis of defects in atomistic simulations, which plays an ever more important role in computational materials science. Some popular and powerful

defect indicators are described. In Section 4 we analyse and compare two concurrent multiscale methods.

The main ingredients of an MD simulation are basically threefold:

- (i) A model is needed for the interaction between the system constituents (e.g. atoms or molecules).
- (ii) Time integration is required to advance the particle trajectories (positions and velocities) from time t to $t + \Delta t$.
 - (iia) Alternatively one may want to solve a stability problem which in an atomistic system requires an algorithm to relax the atomic coordinates to positions of vanishing forces.
- (iii) An ensemble has to be chosen, for which boundary conditions and thermodynamic quantities like temperature, pressure or the number of particles are controlled.

3.1 Force Calculation

Forces are derived from the potential energy U that depends on the positions of all atoms. The description for the calculation of the energy can be based on different physical approximations as described above. The force acting on an atom i is given by taking the derivative of the potential energy with respect to the position vector \mathbf{x}_i of atom i

$$\mathbf{f}_i = -\frac{dU(\mathbf{x})}{d\mathbf{x}_i}, \quad (6)$$

where \mathbf{x} denotes the coordinates of all atoms. Once the force vector \mathbf{f}_i acting on all atoms is known, the Newtonian equation of motion

$$\mathbf{f}_i = m_i \frac{d^2 \mathbf{x}_i}{dt^2}, \quad (7)$$

can be integrated in time t to yield the motion of the atoms in space. The mass of the atom is given by m_i .

3.2 Integrating the Equations of Motion

Equation (7) constitutes a set of second-order ordinary differential equations (ODEs), which can be strongly nonlinear. By converting them to first-order ODEs in the $6N$ -dimensional space of $\{\mathbf{x}_N, \dot{\mathbf{x}}_N\}$, general numerical algorithms for solving ODEs such as the Runge-Kutta method could be applied. However, these general methods are rarely used in practice,

because the existence of a Hamiltonian allows for much simpler and even more accurate integration algorithms.

To represent other thermodynamic ensembles than the *micro-canonical* ensemble for which Equation (7) can be integrated directly, requires that Equation (7) is modified to create a dynamics in phase space that has the desired distribution density of e.g. a *canonical* or a *grand-canonical* ensemble (see e.g. (Frenkel and Smit, 2002)). The time-average of a single-point operator on such a trajectory then approaches the thermodynamic average.

An integrator serves the purpose of propagating particle positions and velocities over small time increments Δt .

$$\mathbf{x}^{3N}(t_0) \rightarrow \mathbf{x}^{3N}(t_0 + \Delta t) \rightarrow \dots \rightarrow \mathbf{x}^{3N}(t_0 + L \Delta t) \quad (8)$$

The time step Δt has to be chosen such that the thermal oscillations of the atoms around their equilibrium positions are resolved in time. A typical frequency of this oscillation is the Debye frequency $\nu_D = c_t/a$, where c_t is the speed of transverse sound waves and a is the lattice parameter. A typical value for metals is $\nu_D \approx 10^{13}$ Hz. This implies that the typical time step for MD simulations has to be on the order of femtoseconds ($=10^{-15}$ s), which generally limits the method to simulations of fast processes such as brittle fracture or high-strain-rate plastic deformation.

Some popular time integration algorithms are the central difference algorithms: Verlet, velocity Verlet or leap-frog. They are shortly introduced below.

• **Verlet algorithm.** Assuming that the $\mathbf{x}^{3N}(t)$ trajectories are smooth, one may perform a third-order Taylor expansion of the positions $\mathbf{x}_i(t_0)$ forward ($\mathbf{x}_i(t_0 + \Delta t)$) and backward ($\mathbf{x}_i(t_0 - \Delta t)$) in time; their sum yields

$$\mathbf{x}_i(t_0 + \Delta t) + \mathbf{x}_i(t_0 - \Delta t) = 2\mathbf{x}_i(t_0) + \ddot{\mathbf{x}}_i(t_0)(\Delta t)^2 + O((\Delta t)^4). \quad (9)$$

Since $\ddot{\mathbf{x}}_i(t_0) = \mathbf{f}_i(t_0)/m_i$ can be evaluated given the atomic positions at $t = t_0$, $\mathbf{x}^{3N}(t_0 + \Delta t)$ in turn may be approximated by,

$$\mathbf{x}_i(t_0 + \Delta t) = -\mathbf{x}_i(t_0 - \Delta t) + 2\mathbf{x}_i(t_0) + \frac{1}{m} \mathbf{f}_i(t_0)(\Delta t)^2 + O((\Delta t)^4). \quad (10)$$

Neglecting the $O((\Delta t)^4)$ term, we obtain a recursion formula to compute $\mathbf{x}^{3N}(t_0 + \Delta t)$. Although velocities are not needed in the recursion, they are often calculated since they are required for analysis of ensemble properties. They can be approximated by

$$\mathbf{v}_i(t_0) \equiv \dot{\mathbf{x}}_i(t_0) = \frac{1}{2\Delta t} [\mathbf{x}_i(t_0 + \Delta t) - \mathbf{x}_i(t_0 - \Delta t)] + O((\Delta t)^2). \quad (11)$$

This algorithm is not only one of the simplest, but also a good choice in general. It is fast, but not particularly accurate for long time steps, such that the forces on all particles must be computed rather frequently. It requires about as little memory as is at all possible. This is useful when very large systems are simulated. Verlet's short-term energy conservation is fair but, more important, it exhibits little long-term energy drift. This is related to the fact that the Verlet algorithm is time reversible and area preserving. In fact, although the Verlet algorithm does not conserve the total energy of this system exactly, strong evidence indicates that it does conserve a pseudo-Hamiltonian approaching the true Hamiltonian in the limit of infinitely short time steps.

• **Velocity-Verlet algorithm.** It starts with $\mathbf{v}^{3N}(t_0)$ and $\mathbf{x}^{3N}(t_0)$. One then evaluates

$$\mathbf{x}_i(t_0 + \Delta t) = \mathbf{x}_i(t_0) + \mathbf{v}_i(t_0)\Delta t + \frac{1}{2} \frac{\mathbf{f}_i(t_0)}{m_i} (\Delta t)^2 + O((\Delta t)^3), \quad (12)$$

with $\mathbf{f}^{3N}(t_0 + \Delta t)$ evaluated from $\mathbf{x}_i(t_0 + \Delta t)$ one gets

$$\mathbf{v}_i(t_0 + \Delta t) = \mathbf{v}_i(t_0) + \frac{1}{2} \left[\frac{1}{m_i} \mathbf{f}_i(t_0) + \frac{1}{m_i} \mathbf{f}_i(t_0 + \Delta t) \right] \Delta t + O((\Delta t)^3), \quad (13)$$

and has advanced by one step. This algorithm requires a little more computing but is very popular since it gives \mathbf{x}^{3N} and \mathbf{v}^{3N} simultaneously.

• **Leap-frog algorithm.** In the leap-frog algorithm, position and velocities are calculated with the same accuracies but are offset by $\Delta t/2$. It starts with $\mathbf{v}^{3N}(t_0 - \Delta t/2)$ and $\mathbf{x}^{3N}(t_0)$. Time integration is then first done on \mathbf{v}

$$\mathbf{v}_i(t_0 + \frac{1}{2}\Delta t) = \mathbf{v}_i(t_0 - \frac{1}{2}\Delta t) + \frac{1}{m_i} \mathbf{f}(t_0)\Delta t + O((\Delta t)^3), \quad (14)$$

followed by integration of \mathbf{x} ,

$$\mathbf{x}_i(t_0 + \Delta t) = \mathbf{x}_i(t_0) + \mathbf{v}_i(t_0 + \frac{1}{2}\Delta t) + O((\Delta t)^3). \quad (15)$$

It can be shown that the leap-frog algorithm produces identical trajectories to the Verlet algorithm besides numerical rounding errors. It therefore has similar properties than the Verlet algorithm but of course provides coordinates and velocities at once.

For the description of *Predictor-Corrector Algorithms* and *Symplectic Integrators* we refer to standard text-books (Frenkel and Smit, 2002; Schlick, 2002; Rapaport, 2004).

3.3 Relaxation Algorithms

Mechanically stable configurations or thermally activated processes are extremely difficult if not impossible to assess with MD methods. Examples for such difficult-to-study processes in the context of fracture would be void formation and coalescence or motion of dislocations in lattices with high Peierls barriers (Marian et al., 2004). For these cases it is usually advisable to map out the energy landscape using relaxation algorithms and then to perform a metadynamics on the basis of such an energy landscape.

Mechanically stable equilibrium configurations correspond to minima of the total energy. Hence it is a most common task in computational materials science and solid state physics to find local or global minima of the potential energy, where a given initial configuration is the point of departure. To solve this task a variety of well-established optimisation methods are available (see e.g. in (Nocedal and Wright, 2006; Leach, 2001; Schlick, 2002)). The optimisation methods generally can be classified according to the highest order derivative used to minimise the (energy) functional. Hence, a non-derivative minimisation method like the simplex method can be considered as zeroth-order method. Zeroth-order methods are rarely used in molecular modelling since first derivatives of the energy (i.e. forces) are usually available and these methods then do not exploit all the available information. In first-order minimisation methods, the gradient of the energy indicates the direction to a minimum, its magnitude measures the steepness of the local slope. These methods are frequently used in molecular modelling. Prominent examples are the steepest descent method and variants of the conjugate gradient (CG) method. For a nice overview we refer to (Shewchuk, 1994). Most recent MD integration-based methods that also fall into this category are described below. Second order methods additionally use the second derivatives and thus the information of the local curvature to locate a minimum. Current state-of-the-art methods like the limited-memory version of the Broyden-Fletcher-Goldfarb-Shanno scheme (l-BFGS) (Nocedal and Wright, 2006) explicitly use only first order derivatives but accumulate information to obtain some approximate representation for the Hessian matrix to determine line search directions. Second order methods are by far not as robust as first order methods and can therefore only be used in molecular modelling if no structural changes occur.

MD-based methods, FIRE. Within the realm of molecular simulations, some methods have been proposed that serve the purpose of energy minimisation, that start out with MD and proceed in removing kinetic energy from the system, termed 'quenching'. This strategy has been successfully

applied in local minimisation as well as in global minimisation. In (Bitzek et al., 2006) a simple, yet powerful MD scheme for structural relaxation was proposed which belongs to this family of minimisers. Different from existing schemes this new algorithm crucially relies on inertia, it has therefore been named the Fast Inertial Relaxation Engine (FIRE). In the original paper the method's functional principle was explained by means of a blind skier searching for the fastest way to the bottom of a valley in an unknown mountain range described by the potential energy landscape $E(\mathbf{x})$ with $\mathbf{x} = (x_1, x_2)$. Assuming that the skier is able to retard and steer, the recommended strategy for the skier is to follow an equation of motion given by:

$$\dot{\mathbf{v}}(t) = 1/m \mathbf{F}(t) - \gamma(t)|\mathbf{v}(t)|[\hat{\mathbf{v}}(t) - \hat{\mathbf{F}}(t)], \quad (16)$$

with the mass m , the velocity $\mathbf{v} = \dot{\mathbf{x}}$, the force $\mathbf{F} = -\nabla E(\mathbf{x})$, and hat denoting unit vector. The recommended strategy is that the skier introduces acceleration in a direction that is 'steeper' than the current direction of motion via the function $\gamma(t)$, if the power $P(t) = \mathbf{F}(t) \cdot \mathbf{v}(t)$ is positive, and in order to avoid uphill motion he simply stops as soon as the power becomes negative. $\gamma(t)$ must be chosen appropriately but should not be too large, because the current velocities carry information about the reasonable 'average' descent direction and energy scale. A discretised version of this equation in combination with an adaptive time step results in a minimisation scheme for multidimensional functions $E(x_1; \dots x_M)$ which is competitive in speed with the fastest optimisers currently available (Bitzek et al., 2006), but has also other important features as we shall demonstrate.

The numerical treatment of the algorithm is simple. Any MD integrator can be used as the basis for propagation of the trajectories due to the conservative forces. The MD trajectories are continuously readjusted by two kinds of velocity modifications: (a) the above-mentioned immediate stop upon uphill motion and (b) a simple mixing of the global velocity and force vectors $\mathbf{v} \rightarrow (1 - \alpha)\mathbf{v} + \alpha\hat{\mathbf{F}}|\mathbf{v}|$ resulting from an Euler-discretisation of the last term in Equation (16) with time step Δt and $\alpha = \alpha_{\text{start}}$. Both, Δt and α , are chosen adaptively on the fly.

The propagation rules for the FIRE algorithm can be summarised as follows (given: initial values for Δt , $\alpha = \alpha_{\text{start}}$ and the global vectors \mathbf{x} and $\mathbf{v} = \mathbf{0}$):

1. MD integrator: calculate \mathbf{x} , $\mathbf{F} = -\nabla E(\mathbf{x})$ and \mathbf{v} using any common MD integrator; check for convergence.
2. calculate $P = \mathbf{F} \cdot \mathbf{v}$.
3. set $\mathbf{v} \rightarrow (1 - \alpha)\mathbf{v} + \alpha|\mathbf{v}|\hat{\mathbf{F}}$.

4. if $P > 0$ and the number of steps since P was negative is larger than N_{\min} , increase the time step $\Delta t \rightarrow \min(\Delta t f_{\text{inc}}, \Delta t_{\text{max}})$ and decrease $\alpha \rightarrow \alpha f_{\alpha}$.
5. if $P \leq 0$, decrease time step $\Delta t \rightarrow \Delta t f_{\text{dec}}$, freeze the system $\mathbf{v} \rightarrow \mathbf{0}$, and set α back to α_{start} .
6. Return to MD.

In relaxation an accurate calculation of the atomic trajectories is not necessary, and the adaptive time step allows FIRE to increase Δt until either the largest stable time step Δt_{max} is reached, or an energy minimum along the current direction of motion ($P < 0$) is encountered. In the latter case the system is instantly frozen ($\mathbf{v} \rightarrow \mathbf{0}$) and the time step is substantially reduced in order to have a smooth restart. A short 'latency' time of N_{\min} MD steps before accelerating the dynamics is important for the stability of the algorithm.

In (Bitzek et al., 2006) it is shown in several benchmark sets that FIRE is very competitive with sophisticated algorithms like the l-BFGS scheme and easily beats even advanced versions of the CG method (e.g. Polak-Ribière). The key advantage of the FIRE algorithm, however, is its extreme robustness. It finds the (local) minima even for extreme structural rearrangements like molecular folding and rotation or for atomic reconstructions in the core of crystalline defects and therefore lends itself ideally as a general purpose minimiser.

3.4 Boundary and initial conditions

Initial conditions. The integration of Newton's equations of motion requires an integrator and initial conditions (IC), namely $\mathbf{x}^{3N}(t = 0)$ and $\dot{\mathbf{x}}^{3N}(t = 0)$, the initial particle positions and velocities.

Generating $\mathbf{x}^{3N}(t = 0)$ for crystalline solids is easily done by a structure generator setting up a perfect crystal or an interface between two crystalline phases. Generating suitable velocity distributions or structures for a liquid or an amorphous solid is significantly more difficult. It can, however, often be circumvented by running the system from an artificial set-up for an extended equilibration time. One can for example melt a crystal and obtain the IC for an amorphous configuration then by quenching from the liquid.

Boundary conditions. Boundary conditions can be classified into two major types: periodic boundary conditions (PBC) and isolated (or free) boundary conditions (IBC). IBC, in which surface atoms exhibit dangling bonds due to a lack of neighbours, are chosen for the analysis of surfaces, clusters and molecules. In addition, there can be extra forces or displace-

ments acting on the boundary atoms, resulting in so-called mechanical boundary conditions.

PBC are intended to mimic bulk solids or liquids, or the cores of very large systems, which are much larger than the simulated number of particles. The particles are contained within a primary simulation volume. This volume is sometimes referred to as the simulation box, unit cell or supercell.

When a particle leaves one side of this volume, it re-enters from the opposite side keeping the number of atoms in the central box constant. Atoms sitting in the vicinity of one side of the box, through periodic repetition of the box, are connected to the atoms on the other side of the box. The simulations therefore proceed as if the primary volume was surrounded in all directions by identical copies of itself to form a quasi-infinite volume. PBC for the two-dimensional case are illustrated in Figure 1. If PBC are used, the case that the cutoff radius is less than half the diameter of the periodic box is of special interest since in that case only the interaction of a given atom with the nearest periodic image of any other atom needs to be considered (*minimum image convention*). This case is displayed in Figure 1, where the dotted box comprises all nearest images of any other atom.

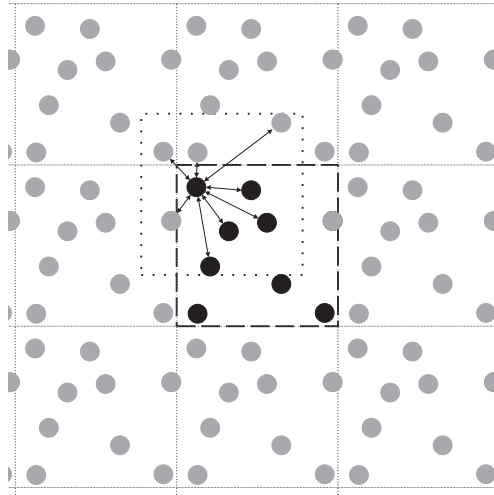


Figure 1. Periodic boundary conditions: the basic simulation volume (drawn in *black*) is repeated in all dimensions. Here, particles in neighbour volumes are drawn in *gray*. Interactions of one atom with its neighbours are indicated with arrows.

The cubic cell is the simplest geometry of an unit cell to visualise and

to program. Of course, any other shape can be chosen provided it fills all of space by translation operations. Five shapes satisfy this condition: the cube (and its close relation, the parallelepiped), the hexagonal prism, the truncated octahedron, the rhombic dodecahedron and the elongated dodecahedron, see e.g. (Leach, 2001).

Using PBC, surface effects can be eliminated from the simulation, but some inherent limitations dictate rules in applying them, see (Pöschel and Schwager, 2005).

- (i) Since each particle or defect has an infinite number of images, there is always an infinite number of interactions with each other particle or defect.
- (ii) If the chosen primary volume is too small, there appear correlations between opposite edges of the primary volume. If the spatial structures are of the same characteristic size as the system itself, a particle may interact directly or indirectly with itself across the primary volume. It is therefore not possible to achieve fluctuations that have a wavelength greater than the length of the cell.

The first item causes problems when long-range forces, such as electrostatic interactions or elastic defect-defect interactions are involved. Sophisticated techniques have been developed, such as Ewald-summation to simulate systems of charged or gravitating particles. For long-range electrostatic interactions it is frequently accepted that some long-range order will be imposed upon the system. Hence, the range of the interactions between particles in the system must generally be taken into account while planning a simulation. No problems will arise if the periodic box is large compared with the range over which the atomic interaction (e.g. of an EAM potential) acts. A box size greater than three times the cut-off radius of the potential is always sufficient. Specific measures have to be taken in the calculation of the forces if shorter box lengths shall be realized.

The second complication listed above is more substantial, since it is inherent to the system and cannot be solved by improved algorithms. Consequently, the basic volume size has to be chosen large enough to avoid undesired artificial correlations. Size scaling studies have to be performed to assess such effects. In favourable cases, the long range interactions of periodic arrays of defects are known and can be subtracted from the total energy of the unit cell.

Boundary conditions that mix IBC and PBC can be required in case that the simulated structure exhibits periodicity in some directions, but not in the others. Typical examples are one-dimensional structures like very long slabs or wires and systems where loads are applied in certain directions.

Mechanical loading through boundary conditions. For the study of the mechanical behaviour of solids like e.g. in fracture processes, a proper definition of boundary conditions and their adequate application are necessary. A simple approach to apply displacement boundary conditions is realized via a domain decomposition, in that a domain is added at the boundary with prescribed stress or displacements. In these domains, atoms are not subject to the dynamics of Newton's equation of motion in an MD simulation; instead, they follow prescribed displacements of the boundaries, see e.g. (Buehler, 2008). Figure 2 schematically displays this approach for the simulation of fracture. A crystalline slab is strained by means of rigid, sufficiently thick boundary layers which are subject to prescribed displacements, whereas the atoms in the interior follow Newton's equations of motion.

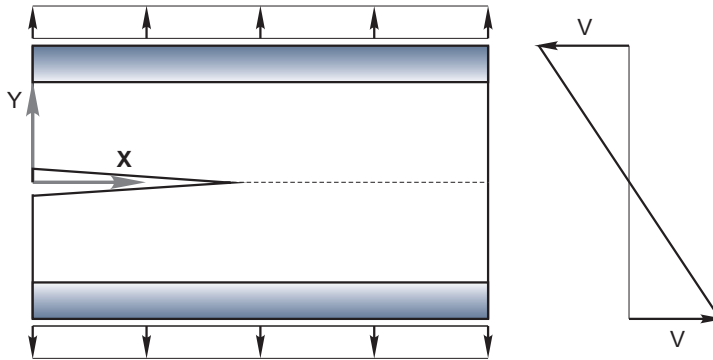


Figure 2. Application of displacement boundary conditions: Atoms in boundary domains (gray-shaded) follow prescribed boundary conditions and are not subject to the equations of motion.

The application of pressure – or generally stress – instead of displacement boundary conditions can be realized by utilizing appropriate ensemble schemes such as the Parinello-Rahman scheme (Parinello and Rahman, 1980).

Since time steps in typical MD simulations are of the order of femtoseconds to keep track of thermal vibrations, the velocity of applied displacement boundary conditions during dynamic straining is necessarily very high. To apply increased mechanical loading, a linear velocity gradient can be established prior to simulation to avoid shock wave generation from the boundaries, see Figure 2, right. However, studying processes at low loading rates is difficult. Sometimes, stress boundary conditions may allow to

simulate somewhat slower loading.

For well controlled loading situations, however, one has to resort to the application of constant displacement boundary conditions and study the system as it evolves in a given field. In the example of Figure 2, the application of a constant displacement u provides a constant (energetic) driving force for the propagation of the crack. With such boundary conditions one can reach the desired case of studying crack propagation at constant energy release rate G .

Since a propagating crack is expected to generate heat, a local temperature control (Finnis et al., 1991), resembling an electronic heat bath for the ions, is applied there. At the outer border of the model the coupling (damping) parameter is gradually increased to prevent reflections from the borders. The model is then first equilibrated at an applied strain corresponding to the Griffith load $G_0 = 2\gamma$. During the equilibration time the crack remains stationary. Thereafter the model is instantaneously strained further to a defined overload ΔG by scaling all displacements. For small overloads $\Delta G = 0.03 - 0.10 G_0$ a short acceleration phase can be detected immediately after loading. This suggests that the crack has finite but very small inertia. After this acceleration phase the crack runs at constant velocity.

3.5 Stable Defects under Load

For the investigation of discrete defects like an individual crack or an individual dislocation one wants to supply the defect with the natural stress and strain fields it also would experience in a realistically large system. This is of course not possible with the rigid straight boundary conditions sketched in Figure 2. Instead a finite size model must be supplied in the border region with the forces or displacements determined from the continuum mechanical stress and strain fields of the defect. For the case of a sharp crack, the model is loaded by first applying the anisotropic linear elastic continuum solution (Sih and Liebowitz, 1968) for a fixed value of the stress intensity factor K to all atoms in the model. As a starting value for K the stress intensity factor K_G (Griffith load) is used. Then all atoms are relaxed to their equilibrium positions by a relaxation algorithm, except for the outermost atoms, which are held fixed at their initial positions. This configuration is then used for further incremental loading or unloading of the model, which is achieved by scaling all displacements and relaxing the whole model at each incremental step. Changes in the atomic configurations at the crack tip are determined by visual inspection of the relaxed configurations. The load at which one or more bonds are broken upon loading is taken as the upper critical stress intensity K_c^+ . (See (Kohlhoff et al., 1991; Gumbsch,

1995) for details about the loading procedure, size scaling tests and the comparison to other methods.) Often periodic boundary conditions are applied along the crack front.

3.6 Visualisation and Analysis of Defects

A key issue in large-scale atomistic simulations is the automatic identification and visualisation of defects and microstructures.

For that purpose algorithms have been developed to identify, highlight and classify typical defect types, see e.g. (Li, 2007). Hence, pictures or movies based on these indicators realize the interface between experiments in the virtual laboratory and the scientist. They enable a transformation of vast data sets to structured information. Since visualisation criteria allow the judicious selection of regions of interest, they also serve a similar purpose as concurrent multiscale methods, namely to compress or reduce large data sets. In the following some of these visualisation criteria are put forward.

Energy method. One way to extract crystal defects from their undisturbed neighbourhood is the energy method. In this method, atoms with an energy value larger than a defined threshold – or within a specified interval – are targeted for display, which exploits the fact that defects exhibit high-energy. The energy method has been successfully applied to visualise microcracks, dislocations, nanovoids and the like. For nanoindentation into (001) fcc aluminium the energy method selects dislocation loops slipping on (111) planes as visualised in Figure 3. Moreover it can be seen that the energy method accounts for the energy difference between free surfaces and bulk material. In order to avoid free surfaces preventing analysis, a subregion of interest is chosen for visualisation. A shortcoming of the energy-method is that it cannot be applied at elevated temperatures. Furthermore, crystalline defects like stacking faults are hard to see using the energy method. In these cases it is favorable to use defect-indicators which take into account the structure of the crystal lattice and its symmetries.

Centrosymmetry parameter. The centrosymmetry parameter (CP) as introduced by (Kelchner et al., 1998) is defined for an fcc atom according to

$$P = \sum_{i=1}^6 |\mathbf{r}_i + \mathbf{r}_{-i}|^2, \quad (17)$$

where vectors \mathbf{r}_i and \mathbf{r}_{-i} correspond to the six pairs of next neighbours lying at opposite sites with respect to the considered atom in the lattice. By definition, the CP is zero for an atom in the bulk of a perfect material subject

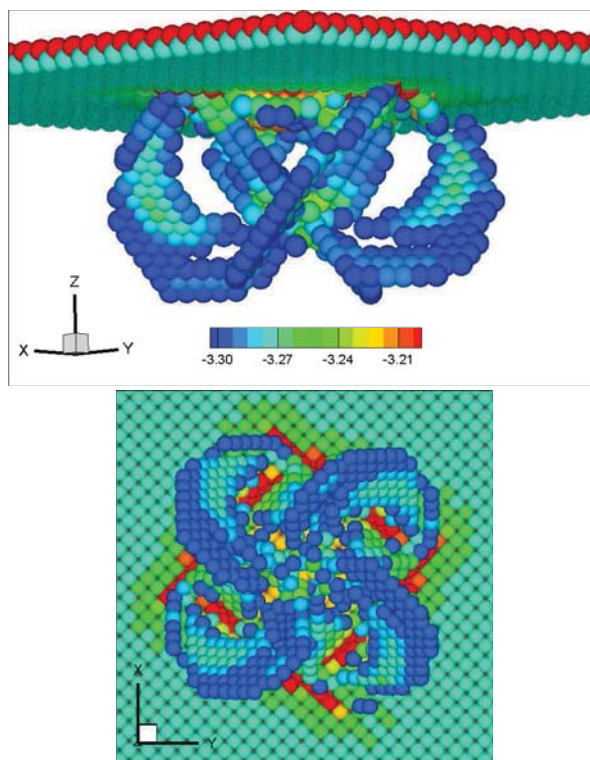


Figure 3. Simulation of nanoindentation into (001) fcc Al at zero temperature: the internal energy criterion extracts the free surface and the dislocation loops.

to purely homogeneous elastic deformations. The deviation of P from zero therefore measures the strength of disturbed centrosymmetry at a lattice site. Opposed to the Energy Method, the CP enables identification and classification of defects like free surfaces, partial dislocations and stacking faults by a certain number.

Since the CP – opposed to the Energy-Method – is related to the crystal’s structure, it is invariant to thermal fluctuations and hence also applicable at finite temperatures.

Slip vector analysis. The slip vector analysis (SVA) was proposed by (Zimmerman et al., 2001) in the context of MD simulation of nanoindentation.

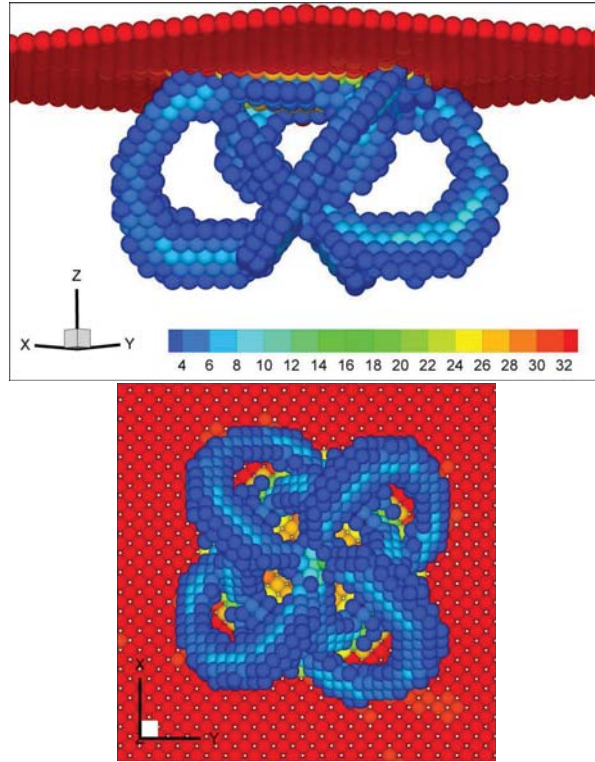


Figure 4. Simulation of nanoindentation into (001) fcc Al: the centrosymmetry parameter extracts the free surface and the dislocation loops.

tion; the slip vector of atom α is defined as

$$\mathbf{s}^\alpha = -\frac{1}{n_s} \sum_{\beta \neq \alpha}^{n_\alpha} \left\{ \mathbf{r}^{\alpha\beta} - \mathbf{R}^{\alpha\beta} \right\}, \quad (18)$$

where n_s is the number of slipped neighbours, n_α is the number of nearest neighbours, $\mathbf{r}^{\alpha\beta}$ and $\mathbf{R}^{\alpha\beta}$ are the vector differences between atom α and atom β in the current and the reference configuration, respectively.

The particular advantage of the SVA over CP is, that Burgers vectors are directly accessible and thus, SVA realizes the bridge to crystallography. Furthermore, the slip vector approach can be applied to very different types of defects in crystalline solids, whereas CP measures only disturbed centrosymmetry.

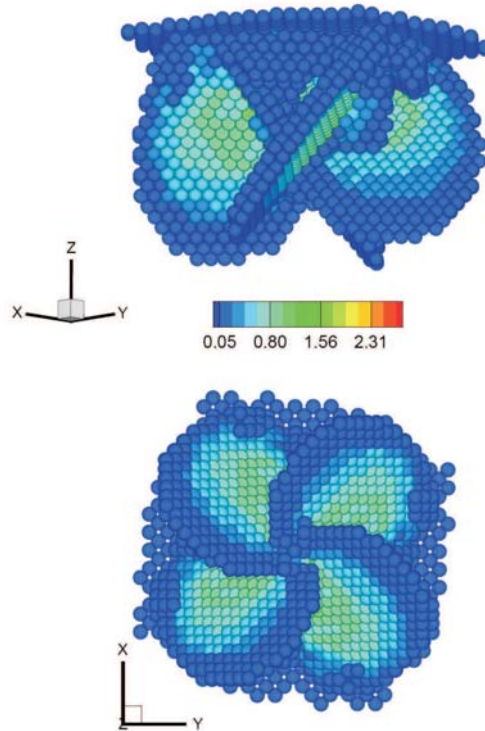


Figure 5. Simulation of nanoindentation into (001) fcc Al: The slip vector analysis, L_2 norm of s^α , extracts the dislocation loops.

Other criteria to identify and visualise defects in crystalline solids are the common neighbour analysis (Honeycutt and Andersen, 1987) and the Bond Angle Analysis (Ackland and Jones, 2006). The bond angle analysis is particularly useful to determine the local coordination, distinguishing fcc, hcp, bcc, and other relatively close-packed structures.

4 Concurrent Multiscale Methods

4.1 Introduction and Classification of Multiscale Methods

Despite the considerable achievements by means of molecular simulations, which have been sped up by the ever more increasing computer power, the range of applicability of atomistic models and methods is still rather lim-

ited in that they have not yet reached the typical time and length scales of engineering applications. The reason is that quite disparate time and length scales have to be considered; for MD the maximum time step is dictated by the frequency of thermal vibrations, hence in the order of femtoseconds, whereas a process like e.g. crack propagation may occur in the order of seconds. The spatial problem is not less demanding, since the length scale at the bottom is in the range of atomic spacings, hence of nanometres, whereas the world of engineering problems lives in the range of some centimetres - and beyond. For that reason many efforts have been undertaken to overcome the time scale and length scale dilemma by *coarse-graining* approaches. The accurate, at best *seamless* information passing from a bottom scale to a corresponding coarse-grained scale –and eventually backwards– is one of the key challenges in computational materials science.

In the following we will consider only the coupling of length scales and not time scales, and doing this, we will moreover restrict to the atomistic-to-continuum scale-coupling at zero temperature. Multiscale methods can be generally separated into two main categories, *hierarchical/sequential* and *concurrent*.

- *Hierarchical or sequential multiscale methods.* In this concept, material information on the atomic scale is generated and passed to a larger length scale. A simple example of this concept is the atomistic calculation of material parameters like elastic constants, thermal expansion coefficients, hardening moduli which are then used as input in continuum constitutive equations. The embedded atom method (EAM) itself can be seen as an example of a hierarchical multiscale method, since the parameters of EAM are determined in ab-initio calculations. Another instance is the identification of parameters in traction-separation laws of atomic debonding, which are employed in cohesive zone finite elements.

This concept of information-passing from a small-scale model to a larger scale model is relatively simple and cheap. Since the material's small-scale response is parametrised for a fixed set of tests to feed the larger-scale model, the larger-scale model cannot account for the full complexity of the material's behaviour in situations far from the test bed, where the model parameters were calibrated. In order to overcome these limitations a second branch of multiscale methods has emerged.

- *Concurrent multiscale methods.* Opposed to the aforementioned class of methods, concurrent multiscale methods explicitly couple models on different length scales. Corresponding computational frameworks allow the running of simulations on disparate length scales in parallel,

i.e. *concurrently*. For that aim the simulation domain is decomposed into different regions, where fully atomistic resolution is retained in critical regions, where deformation strongly varies and where inelastic deformations occur. In regions with weakly varying, purely elastic deformations, continuum constitutive laws are typically employed along with a *coarse-graining* as realized by the finite element method. The overall goal is to achieve a result as accurate as necessary and as effective as possible.

Concurrent multiscale methods are typically used for problem sets where inelastic deformations localise in regions of confined size. These regions typically are embedded into other regions, which deform elastically and which form the largest portion of the entire simulation domain. Since crack propagation is a prominent example in this class, research in the mechanics of fracture has driven the development of concurrent multiscale models and methods, and vice versa.

A number of review articles for concurrent multiscale methods coupling different length scales is available, see e.g. (Ortiz and Phillips, 1999; Miller and Tadmor, 2002; Curtin and Miller, 2003; Miller and Tadmor, 2009), and with a special focus on fracture processes, (Abraham et al., 2000).

In the following we describe two prominent concurrent multiscale methods, the Finite Element Atomistic Method (FEAt) and the Quasicontinuum (QC) Method.

4.2 The Finite Element Atomistic (FEAt) Method

The Finite Element Atomistic (FEAt) Method as introduced in (Kohlhoff, 1990; Kohlhoff et al., 1991) is based on the decomposition of a crystal into generally three different domains as visualised in Figure 6:

- A : a lattice region with fully atomistic resolution, where interatomic potentials are employed.
- C : a continuum region, discretized by finite elements, where a local, but nonlinear continuum constitutive law of anisotropic elasticity is employed.
- T : a transition region in between A and C, where the coupling between the local continuum and the nonlocal lattice is mediated. In this region the framework of Kröner's nonlocal elasticity theory is used. It is a continuum theory, which takes the finite range of internal forces into account and therefore can be seen as a continuation of the lattice, (Kröner, 1963).

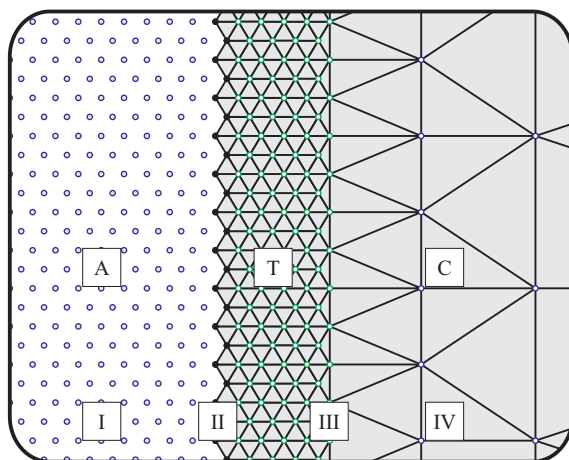


Figure 6. Scale transition scheme in FEAt.

Coupling conditions. The coupling between the atomistic and continuum regions in FEAt is in the first place based on the (i) strong kinematical compatibility and on (ii) stress/force compatibility.

Kinematical coupling. The kinematical compatibility in the transition T region is realized as follows; the transition region where the lattice and the continuum overlap is divided into two zones, II and III, Figure 6. Each zone provides the displacement boundary conditions for the other zone. Zone II, which reduces to a surface in a three-dimensional model, supplies the boundary conditions for the continuum, region IV. The FE nodes on this surface coincide with the atoms of the lattice and move with them. Conversely, in zone III the atoms, which constitute the outer shell of the lattice, are made to move in accord with the FE nodes with which they coincide. A one-to-one correspondence of nodes and atoms throughout the transition region is obtained in this way. This is why this coupling is generally termed *strong compatibility* in the classification of domain decompositions in multiscale models.

The width of zone III must be at least equal to the cut-off length of the potentials used to describe the atomistic core region. Note that the transition zone III must be $2R_{cut}$ thick when the underlying atomistic model is of the EAM type, and thus atomic forces (derivatives of energy) depend on the electron-density at an atom and at an atom's neighbour R_{cut} away, the latter of which depends on a neighbour's neighbour, up to another R_{cut} away.

Force coupling. The design of the model ensures equality of the displacement fields in the lattice and the continuum throughout the transition region, and thus equality of strains at the interface. However, since the use of forces has been explicitly avoided in this coupling scheme, any direct interaction between the stress fields of the two media is prevented. This means that force equilibrium or equality of stress between the lattice and the continuum is not established a priori. Additional conditions are necessary. In FEAt, the coupling condition is on the force level, whereas other concurrent multiscale methods perform the coupling on the energy level. To define these coupling conditions in a consistent fashion, the elastic energy $E = \hat{E}(\varepsilon)$ is expanded into a Taylor series about the state of zero strain under the assumption of zero stress,

$$E(\varepsilon) = E(0) + \left. \frac{\partial E}{\partial \varepsilon_{ij}} \right|_0 + \frac{1}{2} \left. \frac{\partial^2 E}{\partial \varepsilon_{ij} \partial \varepsilon_{kl}} \right|_0 \varepsilon_{ij} \varepsilon_{kl} + \frac{1}{6} \left. \frac{\partial^3 E}{\partial \varepsilon_{ij} \partial \varepsilon_{kl} \partial \varepsilon_{mn}} \right|_0 \varepsilon_{ij} \varepsilon_{kl} \varepsilon_{mn} + \dots \quad (19)$$

For the equality of stresses, the strains and all coefficients in this series must be equal in the atomistic region and in the continuum. Since the strains have been made equal by means of the strong compatibility of displacements, equality of the stresses amounts to the requirement, that the elastic constants of the continuum equal those defined by the interatomic potential in the atomistic region:

$$\mathbb{C}_{ij} = \left. \frac{\partial E}{\partial \varepsilon_{ij}} \right|_0, \quad \mathbb{C}_{ijkl} = \left. \frac{\partial^2 E}{\partial \varepsilon_{ij} \partial \varepsilon_{kl}} \right|_0, \quad \mathbb{C}_{ijklmn} = \left. \frac{\partial^3 E}{\partial \varepsilon_{ij} \partial \varepsilon_{kl} \partial \varepsilon_{mn}} \right|_0. \quad (20)$$

Since the reference state of the series in Equation (19) is a homogeneous deformation, $\varepsilon = 0$, it is indeed permissible to assign to the continuum the second- and higher order elastic constants as defined by Equation (20) and which are derived from the interatomic potential. The first-order elastic constants in the continuum are zero by definition, which imposes the restriction on the potential that it must provide zero stress in a perfect lattice. Within the framework of *local* and *linear* elasticity theory, equilibrium between the lattice and the FE continuum is fulfilled, if terms up to the second order are matched. FEAt accounts for elastic nonlinearity in that, additionally, elastic constants of third order, are adapted as well.

Two approximations in this coupling scheme are made. First, that the series in Equation (19) has to be cut off at some stage. Second, that there is a transition at the discrete interface from interatomic and hence finite-range forces to continuum Cauchy-type stresses. The latter approximation introduces a discontinuity in the nonlocal part of the stress tensor whenever

the strain gradient at the interface does not vanish. As a consequence, the magnitudes of the strain and of the strain gradient at the atomic-continuum influences the quality of the approximation in the model and the applicability to various situations.

Since in the transition region, II and III, finite element mesh nodes and lattice sites as well as their degrees of freedom coincide by virtue of strong compatibility, dispensable degrees of freedom are eliminated by condensation before the solution process. In (Kohlhoff, 1990) it was observed, that the global finite element stiffness matrix is not symmetric, which indicates that the forces are not conservative and hence that the governing equations are not derived from a variational principle. This is due to the fact, that the FEAt model does not start out from a well-defined total energy for the entire coupled problem but rather effects the coupling between the atomistic and continuum domains on the force/stress level as described above.

The fundamental difference between force coupling and energy coupling, its implications and consequences, are analyzed in Section 4.4 where we compare two variants of the QC method.

Application to fracture simulation. The method was used in (Kohlhoff et al., 1991) to analyse crack propagation on cleavage and non-cleavage planes in bcc crystals, using potentials for iron and tungsten as examples. The results explain why both, the $\{100\}$ and $\{110\}$ planes, are cleavage planes in bcc metals and why cleavage on $\{100\}$ is easier than on the close-packed $\{110\}$ planes.

4.3 The Quasicontinuum-Method Based on the Cauchy-Born Rule

The quasicontinuum method is a prominent example of a bottom-up, concurrent multiscale method aiming at a seamless link of atomistic with continuum length scales. This aim is achieved by three main building blocks which are common to each of the existing QC-versions, the QC based on Cauchy-Born elasticity, (Tadmor et al., 1996), (Shenoy et al., 1999), and two variants of a fully nonlocal QC method, (Knap and Ortiz, 2001), (Eidel and Stukowski, 2009):

- (i) a coarse-graining of fully atomistic resolution via kinematic constraints in order to reduce the number of degrees of freedom. Full atomistic resolution is retained where necessary.
- (ii) an approximation of the energy/forces in coarse-grained regions via numerical quadrature which avoids the explicit computation of the site energy of all the atoms.
- (iii) adaptivity, i.e. spatially adaptive resolution, is necessary to automatically balance accuracy and efficiency. It must be directed by a suitable

refinement indicator.

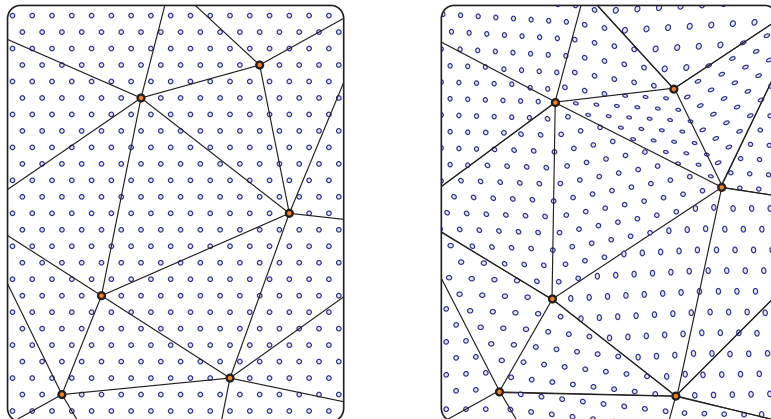


Figure 7. Finite-element discretisation of a crystal in the QC-method in the (left) undeformed configuration and (right) in the deformed configuration. Atoms within elements smoothly follow the mesh nodes by linear interpolation.

To set the stage, we consider a crystal in d -dimensional space consisting of a set $\mathcal{L} \subset \mathbb{Z}^d$ of atoms, that are initially located on a Bravais lattice spanned by lattice vectors $\mathbf{A}_1, \dots, \mathbf{A}_d$. Their coordinates in the initial configuration read $\mathbf{X}_l = \sum_{i=1}^d l^{(i)} \mathbf{A}_i$, $l \in \mathcal{L} \subset \mathbb{Z}^d$. The corresponding atomic coordinates in the current configuration are denoted by vector \mathbf{x}_l .

Upscaling via coarse-graining. In regions of weakly varying elastic deformation it is sufficient to consider the movement of some judiciously selected, *representative* atoms (rep-atoms), $\mathcal{L}_h \subset \mathcal{L}$. Only these atoms keep their independent degrees of freedom, whereas all other atoms, $\overline{\mathcal{L}}_h = \mathcal{L} \setminus \mathcal{L}_h$, are forced to follow via kinematic constraints borrowed from the finite element method: $\mathbf{x}_l = \sum_{j \in \mathcal{L}_h} \mathbf{x}_j \varphi_j(\mathbf{X}_l)$, $l \in \overline{\mathcal{L}}_h$. FE shape functions, $\varphi_j \in \mathcal{L}_h$, exhibit the properties, $\sum_{j \in \mathcal{L}_h} \varphi_j(\mathbf{X}_i) = 1 \ \forall \ i \in \mathcal{L}$ (partition of unity), and, $\varphi_j(\mathbf{X}_{j'}) = \delta_{jj'} \ \forall \ j, j' \in \mathcal{L}_h$ (compact support). The use of (here: linear) shape functions for interpolation requires the generation of a triangulation with representative atoms as mesh nodes. Figure 7 schematically displays the discretisation of the crystal into finite elements.

The interpolation of nodal displacements implicitly introduces a continuum assumption into the QC method. Notwithstanding, this first approx-

imation is purely kinematical in nature, since no constitutive assumptions are made.

The approximation step of discretisation or coarse-graining reduces the number of arguments in the exact total potential, $E^{\text{tot}}(\{\mathbf{x}_i \mid \mathbf{i} \in \mathcal{L}\}) \rightarrow E^{\text{tot}}(\{\mathbf{x}_i \mid \mathbf{i} \in \mathcal{L}_h\}) =: E^{\text{tot},h}$, and thus reduces the number of unknowns in the computation. Both existing QC methods have this approximation step in common, but differ in the way further approximations are made.

Next, we focus on the QC version based on Cauchy-Born elasticity, in Section 4.4 the fully nonlocal QC versions are described and compared.

Efficient energy/force calculation: the local QC. After thinning-out dispensable degrees of freedom via the kinematic constraints in terms of linear finite-element shape functions, the first QC-version as proposed by (Tadmor et al., 1996) accomplishes an efficient energy/force calculation in the continuum region by recourse to the so-called *Cauchy-Born (CB) Rule* -hence QC-CBR- resulting in what is referred to as the *local* formulation of the QC.

The CBR postulates that when a monatomic crystal is subjected to a small linear displacement of its boundary, then all atoms will follow this displacement, see (Born and Huang, 1998), (Ericksen, 1983), (Zanzotto, 1996). The CBR is schematically illustrated in Figure 8 for a crystalline cantilever undergoing elastic bending deformation.

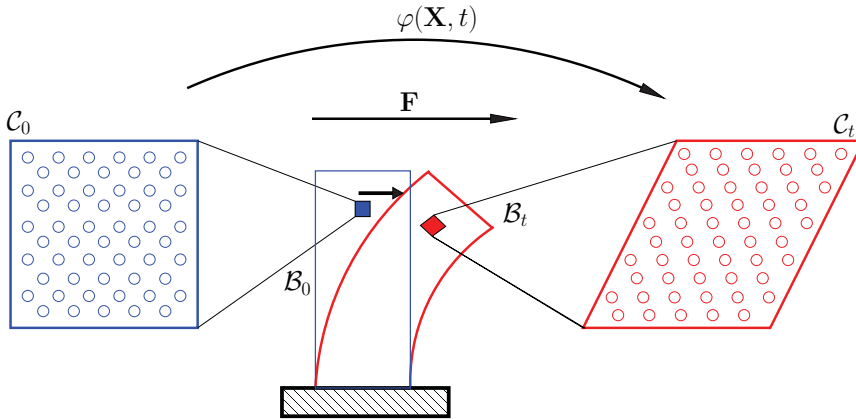


Figure 8. The Cauchy-Born-rule assuming a homogeneous deformation state in small representative volumes.

The CBR is applied in the QC method in that the continuum defor-

mation gradient as a macro-scale quantity is directly mapped to a *uniform* deformation of a small volume on the atomistic or nano-scale. For crystalline solids with a simple lattice structure the assumption of locally homogeneous deformation state implies that every atom in a region subject to a uniform deformation gradient will be energetically equivalent. As a consequence, calculating the energy within a specific finite element can be approximated by computing the energy of only one single atom in the deformed state and multiplying this figure by the number of atoms in the specific finite element. Within the QC-computational framework, the calculation of the CB energy is done separately in a subroutine; for a given deformation gradient \mathbf{F} the lattice vectors in a unit cell with PBC is deformed according to \mathbf{F}

$$\mathbf{a}_i = \mathbf{F} \mathbf{A}_i, \quad (21)$$

where \mathbf{A}_i and \mathbf{a}_i are the lattice vectors in the undeformed configuration and in the deformed configuration, respectively.

The deformed lattice vectors enter the employed potential for energy calculation, such that the CBR enables the free energy of a deformed crystalline body (as a function of lattice vectors) to be expressed alternatively as a function of the deformation gradient \mathbf{F} . The corresponding strain energy density in the element is then given by

$$\mathcal{E} = \frac{E_0(\mathbf{F})}{\Omega_0}, \quad (22)$$

where Ω_0 is the unit cell volume (in the reference configuration) and E_0 is the energy of the unit cell when its lattice vectors are distorted according to \mathbf{F} . Now the total energy of a finite element is this energy density times the element volume, the total energy of the problem is simply the sum of all element energies:

$$E^{tot,h} = \sum_{i=1}^{N_{element}} \Omega_i \mathcal{E}(\mathbf{F}_i), \quad (23)$$

where Ω_i is the volume of element i .

Linear interpolation functions in tetrahedral finite elements require only one single Gauss-point for numerical quadrature and therefore imply a constant deformation gradient per element as visualised in the right of Figure 7. Note, that the locally constant deformation gradient in the finite element matches the assumption of a locally constant deformation gradient in the CBR. As a consequence, the application of the CBR implies that in the energy calculation the summation over the number of lattice sites boils down

to the number of finite elements $N_{element}$, see Equation (23). Since the crystal is in general subject to inhomogeneous deformations, the element-wise constant deformation gradient is an approximation and so is the calculated energy via the CBR. In settings where the deformation is varying slowly and the element size is adequate with respect to the variations of the deformation, this type of energy calculation is sufficiently accurate and very effective.

For a mathematical analysis on the range of validity of the CBR we refer to (Friesecke and Theil, 2002), where it is found that the CBR fails for relatively small elastic deformations. An extension of the classical linear CBR to high order is proposed in (Sunyk and Steinmann, 2003).

Nonlocal QC. In nonlocal regions, which can be eventually refined to fully atomistic resolution, the energy E_α of an atom residing on a mesh node α is calculated by numerical quadrature. Specifically the new approximate energy takes the form

$$E^{tot,h} = \sum_{\alpha=1}^{N_{rep}} n_\alpha E_\alpha(\mathbf{u}_h), \quad (24)$$

where \mathbf{u}_h represents the finite element nodal displacements. The computational saving is that the summation of all the atoms is replaced by a sum over all representative atoms N_{rep} . In the line of numerical quadrature, n_α is the weight function for repatom α which requires for consistency

$$\sum_{\alpha=1}^{N_{rep}} n_\alpha = N. \quad (25)$$

Hence, n_α is the number of atoms represented by atom α , which implies in the limiting case of fully atomistic resolution $n_\alpha = 1$.

Mixed local-nonlocal QC. In order to combine the high accuracy of the nonlocal formulation with the efficiency of the local formulation, the former is employed in critical regions, where atomic scale accuracy is required, where the latter formulation is employed in regions where the deformation is changing relatively slowly on the atomic scale. As a result, the QC-CBR runs both formulations concurrently in a single simulation.

As in the energy-based nonlocal QC, the coupled approach is based on the ansatz that the energy can be approximated by computing only the energy of the repatoms. In the coupled approach however, each repatom is judiciously selected as being either local or nonlocal depending on its

deformation environment. Thus, the repatoms are divided into N_{loc} local repatoms and N_{nonloc} nonlocal repatoms ($N_{loc} + N_{nonloc} = N_{rep}$). Doing this, the total energy is approximated as

$$E^{tot,h} = \sum_{\alpha=1}^{N_{nonloc}} n_{\alpha} E_{\alpha}(\mathbf{u}_h) + \sum_{\alpha=1}^{N_{loc}} n_{\alpha} E_{\alpha}(\mathbf{u}_h). \quad (26)$$

The weights n_{α} for each repatom (local or nonlocal) are determined from a tessellation that divides the body into cells around each repatom. The numerically expensive Voronoi tessellation can be replaced by an approximate Voronoi diagram. The Voronoi cell of repatom α contains a total of n_{α} atoms. Of these atoms, n_{α}^i reside in element i adjacent to repatom α . The total weighted energy contribution of repatom α is then calculated by use of the CBR within each element adjacent to α , hence

$$n_{\alpha} E_{\alpha} = \sum_{i=1}^M n_{\alpha}^i \Omega_0 \mathcal{E}(\mathbf{F}_i), \quad n_{\alpha} = \sum_{i=1}^M n_{\alpha}^i, \quad (27)$$

where \mathcal{E} is the energy density in element i by the CB rule, Ω_0 is the Wigner-Seitz volume of a single atom and M is the number of elements adjacent to α .

The scale transition from fully atomistic resolution to a coarse-grained description is visualised in Figure 9.

The ghost-force problem. QC-CBR inherently exhibits so-called *ghost forces*, defined as spurious forces arising at the interface between local and nonlocal regions. These forces thus follow from the fact that the motion of rep-atoms in the local region subject to the CBR will effect the energy of nonlocal rep-atoms, while the converse may not be true. Hence, this force mismatch stems from different physical assumptions on how atoms interact, which is a compatibility-problem.

There are two different concepts to reduce ghost forces in QC-CBR:

1. Correction by applying a *static correction force field*.
This remedy against ghost forces proposed in (Shenoy et al., 1999) exhibits the drawback that static correction forces are not derivable from a 'correction potential energy', i.e., they are nonconservative. This may lead to serious problems with energy conservation during a molecular-dynamics simulation as reported in (Shimokawa et al., 2004).
2. Correction by *continuation*.
In order to cure the ghost force problem without new shortcomings

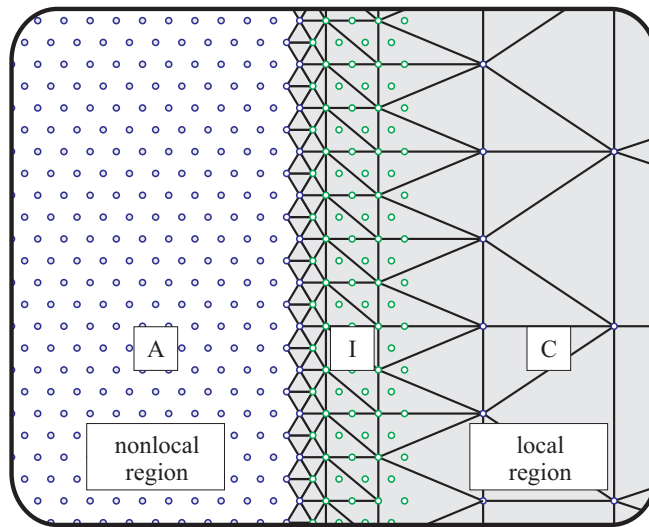


Figure 9. The scale transition scheme in the QC-CBR, where the nonlocal region (A) overlaps in the interface zone (I) with the continuum region (C), which is discretised with finite elements and subject to the CBR.

(Shimokawa et al., 2004) introduced a buffer layer between the two regions of space, where atoms are subject to specific rules concerning how they interact with their local and nonlocal neighbourhood. In a similar spirit is the contribution of (E. et al., 2006), where the approach of local reconstruction schemes is generalised.

Application to fracture. In (Miller et al., 1998a) and (Miller et al., 1998b) the QC-CBR method has been applied to crack tip deformation and is shown to account for both brittle fracture and crack tip dislocation emission. The analysis of a crack propagating into a grain boundary revealed both, migration of the boundary and that the boundary is a source for the emission of dislocations.

4.4 The Fully Nonlocal Cluster-Based Quasicontinuum-Method

A fully nonlocal QC-version (QC-FNL) as proposed by (Knap and Ortiz, 2001) aims to overcome the aforementioned force mismatch between local and nonlocal regions in QC-CBR. For that aim they replace the CBR by a unified nonlocal theory to be described in the following and thus avoid in-

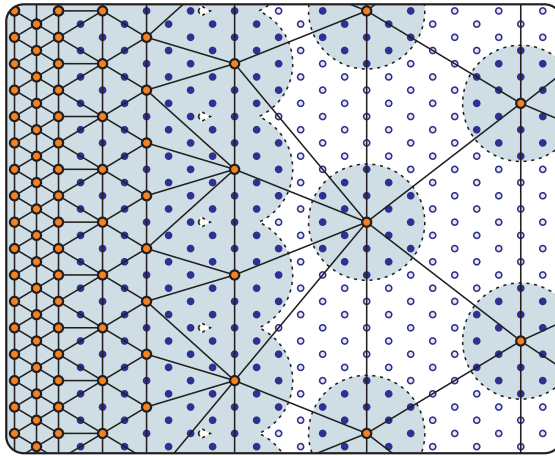


Figure 10. The scale transition scheme in fully nonlocal QC-versions based on force/energy sampling in clusters: the atomistic-continuum coupling is realized in a continuous manner by gradual coarse-graining enabling a seamless scale-transition.

compatibilities of different physical descriptions at discrete interfaces. This then enables the seamless scale transition between fully atomistic resolution and coarse-grained continuum regions. The scale transition in QC-FNL is realized in a continuous manner by gradual coarse-graining, see Figure 10, whereas in QC-CBR it is realized at the discrete interface where different physical models meet, see Figure 9. In the above structure of QC building blocks, (i)–(iii), fully nonlocal QC versions introduce for property (ii) the use of summation rules for the sampling of *forces* or *energies* in spherical clusters, which can be seen as representative crystallites.

Force versus energy sampling in clusters. Even after coarse-graining, the total energy still depends on the site energy $E_{\mathbf{k}}$ of each and every atom \mathbf{k} , $E^{tot,h} = \sum_{\mathbf{k} \in \mathcal{L}} E_{\mathbf{k}}$. Due to the prohibitive computational expense of this task, a second approximation becomes necessary, which is again, like discretisation, a very standard in classical finite element methods: numerical quadrature.

For that purpose Knap and Ortiz (2001) proposed to perform force evaluations no longer at each lattice site in the crystal but to restrict them to sampling clusters. These sampling clusters \mathcal{C}_i are spheres of radius R_c and are chosen to have a mesh node in its centre, see Figures 10 and 11. Hence,

they are defined as $\mathcal{C}_i = \{\mathbf{k} : |\mathbf{X}_k - \mathbf{X}_i| \leq R_c(i)\}$. Note, that the sampling clusters may have different positions, e.g. in the interior of the finite element.

Assuming a pair potential $V = V(\mathbf{r}_{kl})$ with $\mathbf{r}_{kl} = \mathbf{x}_k - \mathbf{x}_l$ and omitting here and in the following the contribution of an external potential V^{ext} , the force acting on node \mathbf{a} reads for **force sampling** in clusters

$$\mathbf{f}_a^h = \sum_{i \in \mathcal{L}_h} n_i \sum_{\mathbf{k} \in \mathcal{C}_i} \mathbf{f}_k \varphi_a(\mathbf{X}_k) = - \sum_{i \in \mathcal{L}_h} n_i \sum_{\mathbf{k} \in \mathcal{C}_i} \left[\sum_{l \in \mathcal{L}} V'(|\mathbf{r}_{kl}|) \frac{\mathbf{r}_{kl}}{|\mathbf{r}_{kl}|} \right] \varphi_a(\mathbf{X}_k). \quad (28)$$

The equilibrium configurations of interest are the minimisers of $E^{\text{tot},h}$, i.e. the solutions of the variational problem:

$$\min_{\{\mathbf{x}_a\}} E^{\text{tot},h} \quad \rightarrow \quad \mathbf{f}_a^h = \mathbf{0} \quad \forall \mathbf{a} \in \mathcal{L}_h. \quad (29)$$

Energy minimisation physically corresponds to solving for the configuration for which at every mesh node \mathbf{a} the sum of forces on each degree of freedom is zero. Based on this fact, Knap and Ortiz (2001) search for the equilibrium by directly working from an approximate expression for the forces according to Equation (28) rather than working from the explicit differentiation of a total energy functional.

In Eidel and Stukowski (2009) however, the sampling is introduced at the energy level, thus

$$E^{\text{QC}} = \sum_{i \in \mathcal{L}_h} n_i \sum_{\mathbf{k} \in \mathcal{C}_i} E_k \approx E^{\text{tot},h}, \quad (30)$$

which yields for **energy sampling** in clusters to the force expression

$$\mathbf{f}_a^h = - \frac{\partial E^{\text{QC}}}{\partial \mathbf{x}_a} = - \sum_{i \in \mathcal{L}_h} n_i \sum_{\mathbf{k} \in \mathcal{C}_i} \frac{1}{2} \sum_{l \in \mathcal{L}} \left[V'(|\mathbf{r}_{kl}|) \frac{\mathbf{r}_{kl}}{|\mathbf{r}_{kl}|} [\varphi_a(\mathbf{X}_k) - \varphi_a(\mathbf{X}_l)] \right], \quad (31)$$

which is the counterpart of Equation (28).

It is worth to note that for energy sampling – as opposed to force sampling – the force expression \mathbf{f}_a^h in Equation (31) is explicitly derived from a well defined total potential E^{QC} , see Equation (30).

Calculation of the weighting factors. In both cases, i.e. for force and energy sampling, factor n_i is the weighting of the force /energy contribution

of cluster \mathcal{C}_i . The cluster weights n_i , $i \in \mathcal{L}_h$, are calculated under the requirement that the summation over all linear interpolation functions must be exact, see Knap and Ortiz (2001), hence

$$\sum_{i \in \mathcal{L}_h} n_i \sum_{\mathbf{k} \in \mathcal{C}_i} \varphi_j(\mathbf{X}_{\mathbf{k}}) = \sum_{\mathbf{k} \in \mathcal{L}} \varphi_j(\mathbf{X}_{\mathbf{k}}) \quad \forall \quad j \in \mathcal{L}_h. \quad (32)$$

The calculation of the weights implies the assumption that the quantity subject to sampling can be exactly approximated if it is linear between the mesh nodes.

When the clusters shrink to the size of the rep-atoms, i.e. $\mathcal{C}_i = \{i\} \forall i \in \mathcal{L}_h$, it holds that $\varphi_{\mathbf{a}}(\mathbf{X}_{\mathbf{k}}) = \delta_{\mathbf{a}\mathbf{k}}$, and the cluster summation rule boils down to a node-based summation rule $\mathbf{f}_{\mathbf{a}}^h = \sum_{\mathbf{k} \in \mathcal{L}_h} n_{\mathbf{k}} \mathbf{f}_{\mathbf{k}} \varphi_{\mathbf{a}}(\mathbf{X}_{\mathbf{k}}) = n_{\mathbf{a}} \mathbf{f}_{\mathbf{a}}$. In this case the weighting factor $n_{\mathbf{k}}$ is the number of atoms represented by rep-atom \mathbf{k} , thus $n_{\mathbf{k}} = \sum_{\mathbf{l} \in \mathcal{L}} \varphi_{\mathbf{k}}(\mathbf{X}_{\mathbf{l}}) \forall \mathbf{k} \in \mathcal{L}_h$, which implies $n_{\mathbf{k}} = 1$ for fully atomistic resolution, i.e. $\mathbf{l} \in \mathcal{L}$, and which ensures that $\sum_{\mathbf{k} \in \mathcal{L}_h} n_{\mathbf{k}} = |\mathcal{L}|$ is fulfilled.

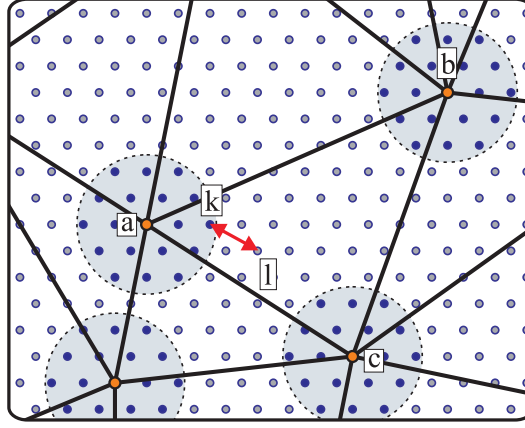


Figure 11. Spherical clusters around mesh nodes for the explicit sampling of forces or energies. The interaction of sampling atom \mathbf{k} inside the cluster with non-sampling atom \mathbf{l} outside the cluster must be symmetric to fulfill Newton's third law.

Is Newton's third law of motion preserved? A critical issue in concurrent multiscale modelling is the coupling of atomistics with a continuum, which is largely due to the general *locality* of continuum constitutive laws and the *nonlocality* of interatomic forces.

In the following we check both sampling schemes to ensure the symmetry of atomic interactions. For that aim we consider the atomic interaction of a sampling atom \mathbf{k} (within the spherical cluster adjacent to mesh node \mathbf{a}) with a non-sampling atom \mathbf{l} as illustrated in Figure 11. It is instrumental to explicitly separate all four force terms (I)-(IV) (see below) for this type of interaction and adhering therein to the lattice statics terms for pair potentials. First, we consider force terms captured by energy sampling. The nonlocal action of energy $E_{\mathbf{k}\leftarrow\mathbf{l}}$ induces a force on atom \mathbf{k} within the cluster, expression (I), and on atom \mathbf{l} outside the cluster, expression (II). These two forces are equal up to the opposite sign, Newton's third law holds, *actio=reactio*. The interaction of atom \mathbf{k} with atom \mathbf{l} is schematically illustrated in Figure 11. Both forces are distributed according to their barycentric coordinates from \mathbf{k} and \mathbf{l} to adjacent nodes \mathbf{a} , \mathbf{b} and \mathbf{c} ; for atom \mathbf{a} the distribution is mediated by factor $[\varphi_{\mathbf{a}}(\mathbf{X}_{\mathbf{k}}) - \varphi_{\mathbf{a}}(\mathbf{X}_{\mathbf{l}})]$ in Equation (31). Moreover, since energy sampling is conceptually restricted to clusters, forces at site \mathbf{k} and site \mathbf{l} due to the energy contribution $E_{\mathbf{l}\leftarrow\mathbf{k}}$, expressions (III) and (IV), are missing in Equation (31); this explains the factor 1/2 therein. It is the function of properly defined weighting factors n_i to account for the energy contribution of non-sampling atoms.

(I) Force on atom \mathbf{k} due to energy $E_{\mathbf{k}\leftarrow\mathbf{l}}$:

$$\tilde{\mathbf{f}}_{\mathbf{k}} = -\frac{\partial E_{\mathbf{k}\leftarrow\mathbf{l}}}{\partial \mathbf{x}_{\mathbf{k}}} = -\frac{1}{2}V'(|\mathbf{r}_{\mathbf{k}\mathbf{l}}|)\frac{\mathbf{r}_{\mathbf{k}\mathbf{l}}}{|\mathbf{r}_{\mathbf{k}\mathbf{l}}|}$$

(II) Force on atom \mathbf{l} due to energy $E_{\mathbf{k}\leftarrow\mathbf{l}}$:

$$\tilde{\mathbf{f}}_{\mathbf{l}} = -\frac{\partial E_{\mathbf{k}\leftarrow\mathbf{l}}}{\partial \mathbf{x}_{\mathbf{l}}} = +\frac{1}{2}V'(|\mathbf{r}_{\mathbf{k}\mathbf{l}}|)\frac{\mathbf{r}_{\mathbf{k}\mathbf{l}}}{|\mathbf{r}_{\mathbf{k}\mathbf{l}}|}$$

(III) Force on atom \mathbf{k} due to energy $E_{\mathbf{l}\leftarrow\mathbf{k}}$:

$$\tilde{\mathbf{f}}_{\mathbf{k}} = -\frac{\partial E_{\mathbf{l}\leftarrow\mathbf{k}}}{\partial \mathbf{x}_{\mathbf{k}}} = -\frac{1}{2}V'(|\mathbf{r}_{\mathbf{k}\mathbf{l}}|)\frac{\mathbf{r}_{\mathbf{k}\mathbf{l}}}{|\mathbf{r}_{\mathbf{k}\mathbf{l}}|}$$

(IV) Force on atom \mathbf{l} due to energy $E_{\mathbf{l}\leftarrow\mathbf{k}}$:

$$\tilde{\mathbf{f}}_{\mathbf{l}} = -\frac{\partial E_{\mathbf{l}\leftarrow\mathbf{k}}}{\partial \mathbf{x}_{\mathbf{l}}} = +\frac{1}{2}V'(|\mathbf{r}_{\mathbf{k}\mathbf{l}}|)\frac{\mathbf{r}_{\mathbf{k}\mathbf{l}}}{|\mathbf{r}_{\mathbf{k}\mathbf{l}}|}$$

The application of the force-based ansatz, Equation (28), gives full account of forces acting on cluster atom \mathbf{k} , summing up expressions (I) and

(III). Contrary to the present ansatz however, Equation (28) does not consider the opposite force acting on atom \mathbf{l} , since \mathbf{l} is not a sampling atom. Briefly, energy-sampling preserves symmetry in atomic interactions whereas force-sampling does not.

It can be equally shown, (Eidel and Stukowski, 2009), that this lack of symmetry in the interaction of sampling atoms with non-sampling atoms implies an asymmetry of the corresponding stiffness matrix, thus indicating nonconservative forces. By contrast, energy sampling leads to strictly symmetric stiffness matrices indicating conservative forces.

The stiffness matrix for energy sampling reads

$$\begin{aligned} \mathbf{k}_{ab}^h &= \frac{\partial^2 E^{\text{QC}}}{\partial \mathbf{x}_a \partial \mathbf{x}_b} \\ &= \sum_{i \in \mathcal{L}_h} n_i \sum_{\mathbf{k} \in \mathcal{C}_i} \frac{1}{2} \sum_{\mathbf{l} \in \mathcal{L}} \left[\varphi_a(\mathbf{X}_{\mathbf{k}}) - \varphi_a(\mathbf{X}_{\mathbf{l}}) \right] \left[\varphi_b(\mathbf{X}_{\mathbf{k}}) - \varphi_b(\mathbf{X}_{\mathbf{l}}) \right] \cdot \\ &\quad \left[\frac{V'(|\mathbf{r}_{\mathbf{k}\mathbf{l}}|)}{|\mathbf{r}_{\mathbf{k}\mathbf{l}}|} \mathbf{1} + \left(\frac{V''(|\mathbf{r}_{\mathbf{k}\mathbf{l}}|)}{|\mathbf{r}_{\mathbf{k}\mathbf{l}}|^2} - \frac{V'(|\mathbf{r}_{\mathbf{k}\mathbf{l}}|)}{|\mathbf{r}_{\mathbf{k}\mathbf{l}}|^3} \right) \mathbf{r}_{\mathbf{k}\mathbf{l}} \otimes \mathbf{r}_{\mathbf{k}\mathbf{l}} \right]. \quad (33) \end{aligned}$$

and for force sampling:

$$\begin{aligned} \mathbf{k}_{ab}^h &= -\frac{\partial \mathbf{f}_a^h}{\partial \mathbf{x}_b} = \sum_{i \in \mathcal{L}_h} n_i \sum_{\mathbf{k} \in \mathcal{C}_i} -\frac{\partial \mathbf{f}_{\mathbf{k}}}{\partial \mathbf{x}_b} \\ &= \sum_{i \in \mathcal{L}_h} n_i \sum_{\mathbf{k} \in \mathcal{C}_i} \varphi_a(\mathbf{X}_{\mathbf{k}}) \sum_{\mathbf{l} \in \mathcal{L}} [\varphi_b(\mathbf{X}_{\mathbf{k}}) - \varphi_b(\mathbf{X}_{\mathbf{l}})] \cdot \\ &\quad \left[\frac{V'(|\mathbf{r}_{\mathbf{k}\mathbf{l}}|)}{|\mathbf{r}_{\mathbf{k}\mathbf{l}}|} \mathbf{1} + \left(\frac{V''(|\mathbf{r}_{\mathbf{k}\mathbf{l}}|)}{|\mathbf{r}_{\mathbf{k}\mathbf{l}}|^2} - \frac{V'(|\mathbf{r}_{\mathbf{k}\mathbf{l}}|)}{|\mathbf{r}_{\mathbf{k}\mathbf{l}}|^3} \right) \mathbf{r}_{\mathbf{k}\mathbf{l}} \otimes \mathbf{r}_{\mathbf{k}\mathbf{l}} \right]. \quad (34) \end{aligned}$$

Summarising, the fully nonlocal QC formulation based on energy sampling, QC-eFNL, exhibits advantages compared to force sampling: sampling at the energy level instead of the force level preserves the variational structure of lattice statics leading to conservative forces, as indicated by symmetric stiffness matrices. More specifically, energy sampling implies the strict symmetry of atomic interactions in all regions, even across the boundary of clusters, whereas force sampling does not in general. Energy sampling also exhibits some numerical advantages. Standard algorithms for the numerical minimisation of functionals like CG methods can directly be applied, since they generally require gradients as well as evaluations of the functional (the energy) itself. Moreover, a minimiser can be found, if the energy exhibits a minimum.

For residual forces observed in QC-eFNL simulations, the following properties have been shown in (Eidel and Stukowski, 2009). Residual forces are conservative in nature; they do not follow from an asymmetry in atomic interactions as a consequence of inconsistent a priori assumptions on how atoms interact; they stem from the error in numerical quadrature and therefore can be reduced (to identically zero) by a sufficiently large cluster size. As such, the present residual forces differ from ghost forces in QC-CBR by source and property, which is the reason why we distinguish by name.

In (Eidel and Stukowski, 2009) QC-eFNL is employed to simulate nanoindentation into (001) aluminium. The simulations have shown the promising capacity of the method to reduce the prohibitive computational expense of fully atomistic resolution (lattice statics) while faithfully simulating the material's response in significant details like the force-depth curve and the load level and locus of dislocation nucleation.

4.5 Other Concurrent Multiscale Methods

There are a variety of concurrent multiscale methods based on a domain decomposition method like FEAt and QC. Here we restrict to name some of them along with key references for the interested reader.

- the Coupling of Length Scale (CLS) Method, (Rudd and Broughton, 1998), (Rudd and Broughton, 2000), (Rudd and Broughton, 2005).
- the Atomistic-to-Continuum Coupling (AtC) method, (Fish et al., 2007).
- the Bridging Scale (BSM) method, (Wagner and Liu, 2003).
- the Coupled Atomistic and Discrete Dislocation (CADD) method, (Shilkrot et al., 2002), (Shilkrot et al., 2004).

4.6 'Learn-On-The-Fly' - LOTF

FEAt and the variants of the QC method deal with the transition from continuum (or coarsened grained) regions of the solid to its fully atomistic resolution, where e.g. EAM potentials are used to describe interatomic forces. As mentioned previously, the parameters in EAM potentials are generally fitted to the results of ab-initio calculations in different settings and are kept fixed for a 'lifetime'. In this sense, EAM potentials themselves can be seen as a hierarchical multiscale method. The method of 'learning on the fly' (LOTF), (Csanyi et al., 2004), is a generalisation of this kind of hierarchical multiscale method in that the parameters of the potential are recalculated and hereby adjusted 'on the fly' for judiciously selected atoms. Doing this, the approach of LOTF ensures a maximum of *accuracy* and *transferability* to the broad variety of simulation settings which cannot be considered in

total in a priori calculations that are performed for a conventional fitting of empirical potential.

According to the general classification, LOTF can also be seen as a concurrent multiscale method. However, since LOTF is adhering to a unified classical force model for the entire system it avoids the 'inherent boundary problem' between different physical models along with inconsistencies which plague many of the concurrent multiscale methods. It is worth mentioning that LOTF has turned out to be quite insensitive to the chosen potentials. It selects simple parametrised potentials and 'augments' it at run time with the necessary extra information, which is computed on the fly by means of quantum calculations.

According to this concept, the flow chart structure of LOTF can be described as follows:

1. *Initialisation*: start out for the physical system in its initial condition with a reasonably parametrised classical potential.
2. *MD predictor, extrapolation*: as in standard molecular dynamics (MD), the chosen potential is used with fixed parameters to predict a system trajectory for a small number of time steps.
3. *Testing*: in the latest configuration, the local validity of the classical potential is assessed on a site by site basis, and a selected subset of atoms is flagged for quantum treatment.
4. *Quantum Mechanics*: use any quantum method (DFT or TB) which provides the desired accuracy to compute the forces on only the selected subset of atoms.
5. *Force Fitting*: the parameters of the classical potential are tuned locally around the selected atoms until it reproduces the accurate force.
6. *MD corrector: interpolation*: return the state of the system to that before the extrapolation and rerun the dynamics, interpolating the potential parameters between the old and the new values.
7. *Return to 2.*

The successful application of LOTF critically depends on the proper choice of criteria that will correctly identify regions for quantum treatment.

Recent application examples of the LOTF method include studies of dynamic crack propagation (Kermode et al., 2008) which will be discussed in some more details later. A review of recent progress in the methodology of hybrid quantum/classical (QM/MM) atomistic simulations for solid-state systems can be found in (Bernstein et al., 2009). In this reference a unified terminology is defined into which the various and disparate schemes fit, based on whether the information from the QM and MM calculations is combined at the level of energies or forces. Moreover, the pertinent issues for achieving 'seamless' coupling and the advantages and disadvantages of

the proposed schemes are discussed. Finally, the applications and scientific results obtained to date are summarised.

5 Atomistic Aspects of Fracture

Fracture is a phenomenon which spans over many length scales. The macroscopic dimensions of the crack and the specimen determine the intensity of the stress concentration at the crack tip and are equally important as the microstructure of the material, which provides preferred fracture paths. Ultimately, fracture reduces to the breaking of atomic bonds, which in the case of brittle fracture occurs at an atomically sharp crack tip (Lawn, 1993; Clarke, 1992). In a perfectly brittle material, the crack moves by no other process than the breaking of individual bonds between atoms. Nevertheless, traditional theory of brittle fracture processes does not focus on individual atomic bonds but resorts to the treatment of Griffith (Griffith, 1921), which is based on continuum thermodynamics. Following Griffith, one may regard the static crack as a reversible thermodynamic system for which one seeks equilibrium. The equilibrium condition leads to the so-called Griffith criterion, which balances the crack driving force and the material resistance against fracture. The crack driving force can be expressed as the stress intensity factor K while the material resistance against fracture for the perfectly brittle case must be at least the surface energy of the two fracture surfaces. With the implication of thermodynamic equilibrium, the Griffith picture provides a reference value K_G for the analysis of the crack driving forces. It however cannot explain why and how fracture proceeds.

From an atomistic point of view, one immediately identifies the material's resistance against fracture with the forces needed to break the crack tip bonds successively. The first atomistic studies of fracture (Thomson et al., 1971) showed that the discrete bond breaking event manifests itself in a finite stability range, which was attributed to the discreteness of the lattice and called the "lattice-trapping" effect. Lattice trapping causes the crack to remain stable and not to advance/heal until loads K^+ or K^- , somewhat larger/smaller than the Griffith load are reached. Other influences of the atomic nature of a crack have recently been summarised in a series of articles in the MRS Bulletin (Selinger and Farkas, 2000). Consequences of the lattice trapping have been reviewed (Gumbsch and Cannon, 2000; Gumbsch, 2001) and only two particularly important and enlightening aspects of the lattice trapping, crack propagation anisotropy and the production of metastable fracture surfaces, are discussed below.

5.1 Lattice Trapping and the Directional Cleavage Anisotropy

Silicon is reported to have two principal cleavage planes: $\{111\}$ planes, usually the easy cleavage planes, and $\{110\}$ planes (Michot, 1988; George and Michot, 1993), the planes of easy cleavage in polar III-V semiconductors. The most accurate constant-K experiments (Michot, 1988) seem to show that $\{110\}$ planes have a slightly lower fracture toughness than $\{111\}$ planes. For both cleavage planes, the measured fracture toughness gives surface energies ($\gamma_{110} = 2.3\text{J/m}^2$, $\gamma_{111} = 2.7\text{J/m}^2$) which are significantly larger than the values calculated atomistically using density functional theory (DFT) based quantum mechanical methods ($\gamma_{110} = 1.7\text{J/m}^2$, $\gamma_{111} = 1.4\text{J/m}^2$) (Pérez and Gumbsch, 2000a).

Propagation direction anisotropy has been observed for both cleavage planes. The preferred propagation direction is along $\langle 110 \rangle$ on both cleavage planes (Michot, 1988; George and Michot, 1993). On the $\{111\}$ fracture surface, the anisotropy with respect to propagation direction is minimal. In contrast, cleavage on the $\{110\}$ plane is extremely anisotropic. Propagation along the $\langle 110 \rangle$ direction results in nearly perfectly flat fracture surfaces (Michot, 1988; George and Michot, 1993). Attempts to achieve propagation in the $\langle 001 \rangle$ direction, perpendicular to the preferred direction, have not been successful because the crack deflects onto $\{111\}$ planes (George and Michot, 1993; Cramer et al., 2000). The relation of the calculated surface energies and elastic anisotropy cannot account for this deviation of the crack (Pérez and Gumbsch, 2000b) and an atomistic investigation therefore is attractive.

DFT calculations of the crack tip stability, the anisotropy in fracture behaviour with respect to the propagation direction on the $\{110\}$ plane was explained as a consequence of a difference in lattice trapping for the different propagation directions (Pérez and Gumbsch, 2000b). A $\{110\}$ crack propagating in the "easy" $\langle 110 \rangle$ direction (see Figure 12 (left)) continuously opens successive bonds at the tip of the crack. This continuous process leads to a relatively small trapping, and it can be argued that the trapping may further decrease as the size of the model (specimen) is increased. In contrast, a crack driven in the "difficult" $\langle 001 \rangle$ direction on the $\{110\}$ plane, displayed in Figure 12 (right), shows a clearly discontinuous bond breaking. Figure 13 shows the bond distances of the crack tip bonds (labeled "B" in Figure 12) for both systems. Further analysis of this discontinuous bond breaking process shows that it is mainly a result of the relaxation of the six or eight atoms around the crack tip and connected with a significant load sharing between the crack tip bond and the one above (Pérez and Gumbsch, 2000a). Comparing both the loading and unloading processes, it is seen that the discontinuous bond breaking is also connected with a

larger lattice trapping range (Pérez and Gumbsch, 2000b). This difference in the trapping effectively destabilises the $\{110\}$ crack propagation in the $\langle 001 \rangle$ direction against deflection onto an inclined $\{111\}$ cleavage plane. Thereby lattice trapping appears to provide the only reasonable explanation for the experimentally observed cleavage anisotropy with respect to the propagation direction for the $\{110\}$ cracks in silicon.

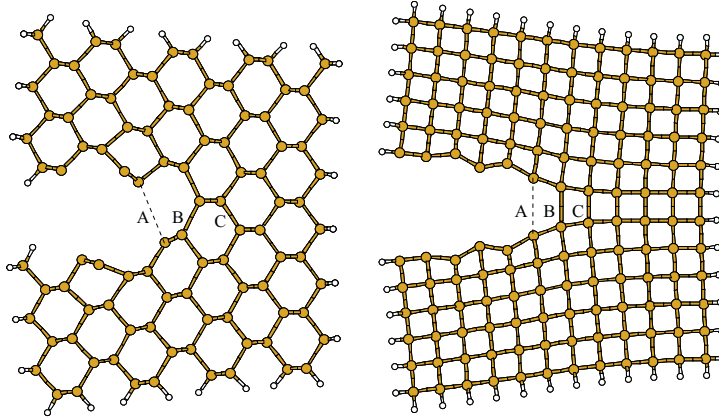


Figure 12. Sequence of bond breaking events during fracture in silicon for different orientations as given in the text.

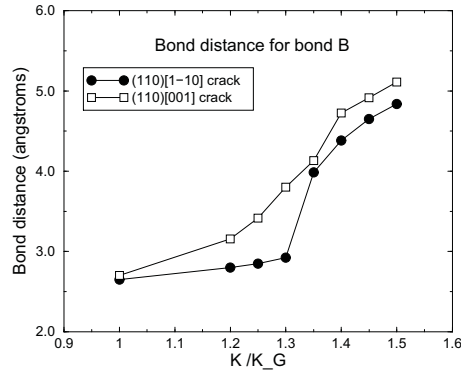


Figure 13. Bond distances of crack tip bonds "B" in Figure 12 during loading.

The same type of propagation anisotropy has recently been found in DFT

calculations of the cleavage of diamond (Pastewka et al., 2008). Similarly an anisotropy with respect to the propagation direction had also been predicted for the cleavage of tungsten single crystals (Kohlhoff et al., 1991; Riedle et al., 1996; Gumbsch et al., 1998)

5.2 Metastable Fracture Surfaces

A crack which experiences significant trapping can be loaded above the Griffith load and still does not propagate. Upon increasing the load, the crack is expected to eventually take the path that is associated with the lowest energy barrier to propagation. With trapping this path is not necessarily the one which leads to the surface of lowest energy. A very prominent example of such behaviour is the surface reconstruction after cleavage of silicon $\{111\}$ planes. Low temperature cleavage ($\leq 600\text{K}$) produces the 2×1 Pandey π -bonded chain reconstruction (Pandey, 1981), while high temperature annealing gives the so called 7×7 reconstruction. This latter structure is energetically more favourable but not directly accessible through the fracture process.

Atomistically simulating the fracture of the intermetallic alloy B2-NiAl (Ludwig and Gumbsch, 1998), using an embedded atom potential specifically developed for B2-NiAl (Ludwig and Gumbsch, 1995), it was observed that a $\{100\}$ crack driven in a $\langle 001 \rangle$ direction did not cleanly separate the adjoining (200) Ni and Al layers. It instead took a zig-zag path which split the Al (200) plane directly in front of the crack tip and deposited every second row of atoms on the upper and the lower fracture surfaces, respectively (see Figure 14). This result would not be so remarkable if the surface energy of the half-occupied Al (100) surface (1.86 J/m^2) were not higher than the average for the Ni and Al terminated surfaces (1.76 J/m^2) (Ludwig and Gumbsch, 1998). The crack had obviously been overloaded to the extent that it could release enough elastic energy so as to create the high-energy half-occupied surfaces. It did so because the energy barrier for this process (0.18 J/m^2) is lower than the trapping barrier for the ideal surfaces.

In this example of NiAl, the crack is creating two identical half-occupied fracture surfaces instead of the asymmetric arrangement of the two surfaces being fully occupied by Ni and Al, respectively. Similar half-occupied surfaces would also be expected in equilibrium for an ionic material where the asymmetric fully occupied surfaces would be oppositely charged (Tasker, 1986). With this analogy in mind, one may search for even more pronounced trapping effects in ionic materials where the crack faces the problem of sorting out the charges.

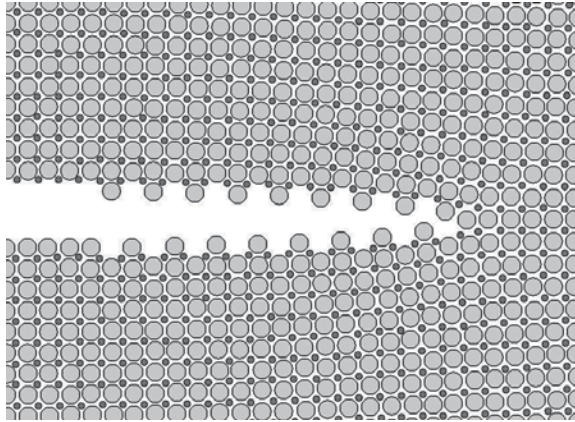


Figure 14. Rough fracture surface of B2-NiAl created during dynamic fracture.

6 Dynamics of Brittle Crack Propagation

The fracture of materials can be a dynamic process, particularly in the final stage of supercritical propagation. Although this final stage of fracture might at first seem almost irrelevant, closer consideration shows that it is precisely the dynamics of the brittle crack which competes with the rate-dependent plasticity in the near tip region to determine whether a propagating crack can ever be stopped. The dynamic crack propagation has therefore recently attracted significant attention.

The first set of atomistic investigations of dynamically moving cracks were directed towards understanding the steady state propagation, crack speed and the onset of dynamic instabilities. Analytical atomistic studies (Marder and Gross, 1995) on simplified one- and two-dimensional structures show that the dynamically propagating crack can only access a limited velocity regime. After initiation, crack tip speed immediately reaches about 20% of the Rayleigh wave velocity and approaches a branching instability at about half the Rayleigh wave velocity (Marder and Gross, 1995). The instability manifests itself in the breaking of bonds at the flanks of the crack before the breaking of the next bond in the propagation direction and is interpreted as a branching instability.

MD simulations (Gumbsch et al., 1997) of the propagation of a mode I crack with a straight crack front and a short periodic length along the crack front (quasi-two-dimensional geometry) essentially confirm the analytical results. They confirm a lower band of forbidden velocities for the straight

crack and also reveal an upper critical velocity. The upper critical velocity for the mode I crack is shown to strongly depend on the non-linearity of the atomic interaction. For harmonic snapping spring force laws (Gumbsch et al., 1997) and for open crystal structures with strong directional bonds (Hauch et al., 1999; Swadener et al., 2002) the velocities can be almost as high as the Rayleigh wave velocity, the relativistic upper limit. Only 40% of the Rayleigh wave velocity is reached for closed packed crystals and more realistic non-linear atomic interactions (Gumbsch et al., 1997). Up to 50% of the shear wave speed is reached in the more complex quasicrystalline structures (Mikulla et al., 1998).

Increasing temperature reduces this band of forbidden velocities and successively allows cracks to also propagate at lower speeds (Holland and Marder, 1999; Rudhart et al., 2003). In amorphous or quasicrystalline structures, increasing the temperature may also lead to a change in crack propagation mechanism from the propagation of a distinct crack tip to crack propagation by successive opening of pores or daughter cracks in front of the main crack and their backward propagation (Falk and Langer, 1998, 2000; Rudhart et al., 2003). This of course drastically reduces the crack propagation speed.

Above the critical velocity, the MD simulations reveal a rich set of different types of instabilities depending on the crystallographic orientation of the crack and on the crystal structure (Gumbsch et al., 1997; Hauch et al., 1999; Mikulla et al., 1998). The generation of cleavage steps and dislocation emission are usually observed at lower overloads, while crack bifurcation was only observed at the highest overloads. Dislocation emission usually leads to a pronounced change in crack propagation direction.

Surprisingly, a different dynamic instability was found in silicon on the (111) cleavage plane not at high speeds but rather at low speeds. In (Kermode et al., 2008) LOTF was applied to investigate this low-speed crack propagation instability using quantum-mechanical hybrid, multi-scale modelling and single-crystal fracture experiments. The simulations predict a crack-tip reconstruction that makes low-speed crack propagation unstable to deflect towards just one of the two crack faces on the (111) cleavage plane, which is conventionally thought of as the most stable cleavage plane. An asymmetrical crack tip reconstruction was found to be responsible for this reconstruction. A small energy barrier needs to be overcome to assess this crack tip reconstruction. Corresponding experiments confirm this instability prediction at a range of low speeds, using an experimental technique designed for the investigation of fracture under low tensile loads.

Further simulations (Kermode et al., 2008) also explain why, at moderately high speeds crack propagation on the (110) cleavage plane becomes

unstable and deflects onto (111) planes, as previously observed experimentally.

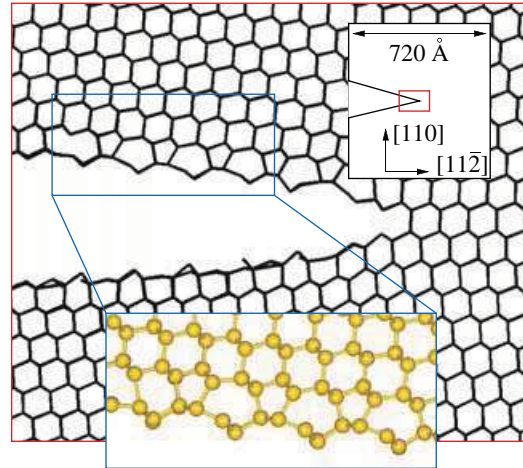


Figure 15. Propagation of the (111)[110] crack in silicon, using the LOTF scheme and the SIESTA code as quantum engine. Brittle fracture propagation on a (111) cleavage plane is correctly predicted.

Large scale MD simulations have recently confirmed continuum mechanical analysis (Gao et al., 1999) on the fact that mode II cracks just like edge dislocations (Gumbsch and Gao, 1999) are not bound by the shear wave speed as an upper limit (Gao et al., 2001). They show a transition to intersonic propagation via the nucleation of a daughter crack out of a subsonic mother crack. Large-scale MD simulations on dynamic fracture under mode I conditions have revealed that the properties of atomic bonds in the vicinity of the crack tip determine the maximum crack propagation speed (Buehler et al., 2003). By taking into account that atomic bonds under high strains, as they occur around crack tips, show non-linear elastic behaviour, it was found that the the maximum velocity may deviate significantly from that calculated by the global linear elastic properties of the material. At large strains, metallic bonds typically weaken and thus show a reduced stiffness before they break. In polymers, in contrast, the material typically becomes stiffer at large tensile strain, because the long-chained molecules are stretched. In (Buehler et al., 2003) it could be shown that the local elastic properties in a certain critical volume around the crack tip governs the dynamic fracture, rather than the global material properties.

Hence, if the material stiffens under tensile load, the crack may become supersonic compared to the global speed of sound in the material, while it is locally still subsonic.

7 Summary

The flexibility of MD methods makes them a versatile tool for studying a wide range of materials phenomena, and in particular fracture in dynamic situations. Because the size of the samples under consideration is considerably larger than in *ab initio* simulations, MD simulations can be used to compare the instability of a crack tip against propagation with its instability against shear. Since the latter process leads to the generation of dislocations, the fracture behaviour is no longer pure cleavage, but is accompanied by some plasticity. In this article the fundamentals of classical MD methods have been introduced, to demonstrate the possibilities and also the limitations of atomistic method. Furthermore, scale bridging methods have also been included which will in the future allow the community to study fracture in larger volumes and possibly on larger time scales than classical MD allows for.

Some applications of MD methods to studying and understanding fracture processes have been briefly mentioned to demonstrate the power of this method. In particular, MD simulations contributed to the understanding of brittle crack advance as a process of continuous bond breaking, which is necessarily described incompletely by any continuum method. Due to the limitations of MD methods to short time scales, dynamic fracture is a fertile field for investigations, but also the conditions for dislocation nucleation at crack tips and the interaction of propagating cracks with dislocations or pores can be studied at the atomic scale, (Zhou et al., 1996; Bitzek, 2006; Bitzek and Gumbsch, 2007).

This article thus provides an introduction to atomistic simulation methods and their application to fracture processes. Literature for in depth reading is also provided.

Bibliography

- F. F. Abraham, N. Bernstein, J. Q. Broughton, and D. Hess. Dynamic fracture of silicon: Concurrent simulation of quantum electrons, classical atoms, and the continuum solid. *MRS Bull.*, 25/5:27, 2000.
- G. J. Ackland and A. P. Jones. Applications of local crystal structure measures in experiment and simulation. *Phys. Rev. B*, 73(5), 2006. ISSN 1098-0121.

- N. Bernstein, J. R. Kermode, and G. Csanyi. Hybrid atomistic simulation methods for materials systems. *Rep. Prog. Phys.*, 72(2), 2009. ISSN 0034-4885.
- E. Bitzek. *Atomistic simulation of dislocation motion and their interaction with crack tips and voids*. PhD thesis, University of Stuttgart, Germany, 2006.
- E. Bitzek and P. Gumbsch. Atomistic simulations of dislocation - crack interaction. In W. E. Nagel, W. Jäger, and M. Resch, editors, *High Performance Computing in Science and Engineering 06*, pages 127–135, Berlin, 2007. Springer Verlag.
- E. Bitzek, P. Koskinen, F. Gähler, M. Moseler, and P. Gumbsch. Structural relaxation made simple. *Phys. Rev. Lett.*, 97(17), 2006. ISSN 0031-9007.
- M. Born and K. Huang. *Dynamical Theory of Crystal Lattices*. Oxford University Press, 1998.
- M. J. Buehler. *Atomistic Modeling of Materials Failure*. Springer, 2008.
- M. J. Buehler, F. F. Abraham, and H. Gao. Hyperelasticity governs dynamic fracture at a critical length scale. *Nature*, 426:141–146, 2003.
- D. R. Clarke. *Semiconductors and Semimetals, edited by K.T. Faber and K. Malloy, Academic Press.*, page 79., 1992.
- T. Cramer, A. Wanner, and P. Gumbsch. Energy dissipation and path instabilities in dynamic fracture of silicon single crystals. *Phys. Rev. Lett.*, 85:788, 2000.
- G. Csanyi, T. Albaret, M.C. Payne, and A. De Vita. "Learn on the fly": A hybrid classical and quantum-mechanical molecular dynamics simulation. *Phys. Rev. Lett.*, 93(17), OCT 22 2004. ISSN 0031-9007. doi: 10.1103/PhysRevLett.93.175503.
- W. A. Curtin and R. E. Miller. Atomistic/continuum coupling in computational materials science. *Model. Simul. Mater. Sci. Eng.*, 11(3):R33–R68, 2003. ISSN 0965-0393.
- V. S. Deshpande, A. Needleman, and E. Van der Giessen. Discrete dislocation plasticity modeling of short cracks in single crystals. *Acta Mater.*, 51:1–15, 2003.
- B. Devincre and S. G. Roberts. Three-dimensional simulation of dislocation-crack interactions in b.c.c. metals at the mesoscopic scale. *Acta Mater.*, 44:2891–2900, 1996.
- W. E., J. Lu, and J. Yang. Uniform accuracy of the quasicontinuum method. *Phys. Rev. B*, 74(21), 2006. ISSN 1098-0121.
- B. Eidel and A. Stukowski. A variational formulation of the quasicontinuum method based on energy sampling in clusters. *J. Mech. Phys. Solids*, 57(1):87–108, 2009.

- F. Ercolessi and J. B. Adams. Interatomic potentials from first-principles calculations: the force-matching method. *Europhys. Lett.*, 26:583–588, 1994.
- J. Ericksen. *The Cauchy and Born Hypotheses for Crystals*. Defense Technical Information Center, 1983.
- M. L. Falk and J. S. Langer. Dynamics of viscoplastic deformation in amorphous solids. *Phys. Rev. E*, 57:7192, 1998.
- M. L. Falk and J. S. Langer. From simulation to theory in the physics of deformation and fracture. *MRS Bull.*, 25/5:40, 2000.
- M. W. Finnis, P. Agnew, and A. J. E. Foreman. Thermal excitations of electrons in energetic displacement cascades. *Phys. Rev. B*, 44:567, 1991.
- J. Fish, M. A. Nugeghally, M. S. Shephard, C. R. Picu, S. Badia, M. L. Parks, and M. Gunzburger. Concurrent AtC coupling based on a blend of the continuum stress and the atomistic force. *Comp. Meth. Appl. Mech. Eng.*, 196(45-48):4548–4560, 2007. ISSN 0045-7825.
- D. Frenkel and B. Smit. *Understanding Molecular Simulation: From Algorithms to Applications*. Academic Press, 2002.
- G. Friesecke and F. Theil. Validity and failure of the Cauchy-Born hypothesis in a two-dimensional mass-spring lattice. *J. Nonlinear Sci.*, 12(5): 445–478, 2002. ISSN 0938-8974.
- H. Gao, Y. Huang, P. Gumbsch, and A. J. Rosakis. On radiation-free transonic motion of cracks and dislocations. *J. Mech. Phys. Solids*, 47: 1941, 1999.
- H. Gao, Y. Huang, and F. F. Abraham. Continuum and atomistic studies of intersonic crack propagation. *J. Mech. Phys. Solids*, 49:2113, 2001.
- A. George and G. Michot. Dislocation loops at crack tips - nucleation and growth - an experimental-study in silicon. *Mater. Sci. Eng. Ag*, 164:118, 1993.
- A. A. Griffith. Phenomena of rupture and flow in solids. *Philos. Trans. R. Soc. London, Ser. A*, 221:163., 1921.
- P. Gumbsch. An atomistic study of brittle fracture: Towards explicit failure criteria from atomistic modelling. *J. Mater. Res.*, 10:2897–2907, 1995.
- P. Gumbsch. *Materials Science for the 21st Century, vol. A*, The Society of Materials Science, JSMS, Japan, 2001.
- P. Gumbsch and R. M. Cannon. Atomistic aspects at brittle fracture. *MRS Bull.*, 25/5:15., 2000.
- P. Gumbsch and H. Gao. Dislocations faster than the speed of sound. *Science*, 283:965, 1999.
- P. Gumbsch, S.-J. Zhou, and B. L. Holian. Molecular dynamics investigation of dynamic crack stability. *Phys. Rev. B*, 55:3445, 1997.

- P. Gumbsch, J. Riedle, A. Hartmaier, and H. F. Fischmeister. Controlling factors for the brittle-to-ductile transition in tungsten single crystals. *Science*, 282:1293, 1998.
- W.A. Harrison. *Solid state theory*. Courier Dover Publications, 1980.
- J. A. Hauch, D. Holland, M. P. Marder, and H. L. Swinney. Dynamic fracture in single crystal silicon. *Phys. Rev. Lett.*, 82:3823, 1999.
- P. Hohenberg and W. Kohn. Inhomogeneous electron gas. *Phys. Rev.*, 136(3B):B864–B871, 1964.
- D. Holland and M. Marder. Cracks and atoms. *Adv. Mater.*, 11:793, 1999.
- J. D. Honeycutt and H. C. Andersen. Molecular dynamics study of melting and freezing of small lennard-jones clusters. *J. Phys. Chem.*, 91:4950–4963, 1987.
- M. E. Kassner, S. Nemat-Nasser, Z. G. Suo, G. Bao J. C. Barbour, L. C. Brinson, H. Espinosa, H. J. Gao, S. Granick, P. Gumbsch, K. S. Kim, W. Knauss, L. Kubin, J. Langer B. C. Larson, L. Mahadevan, A. Majumdar, S. Torquato, and F. van Swol. New directions in mechanics. *Mech. Mater.*, 37:231–259, 2005.
- C. L. Kelchner, S. J. Plimpton, and J. C. Hamilton. Dislocation nucleation and defect structure during surface indentation. *Phys. Rev. B*, 58:11085–11088, 1998.
- J. R. Kermode, T. Albaret, D. Sherman, N. Bernstein., P. Gumbsch, M.C. Payne, G. Csanyi, and A. De Vita. Low-speed fracture instabilities in a brittle crystal. *Nature*, 455(7217):1224–U41, 2008. ISSN 0028-0836.
- J. Knap and M. Ortiz. An analysis of the quasicontinuum method. *J. Mech. Phys. Solids*, 49(9):1899–1923, 2001. ISSN 0022-5096.
- S. Kohlhoff. *Ein Verfahren für die Rechnermodellierung eines atomistischen Gitterbereiches, umgeben von einem Finite-Elemente-Kontinuum, und seine Anwendung auf Rissfortschrittsprozesse in kubisch-raumzentrierten Metallen*. PhD thesis, MPI for Metal Research, Stuttgart, 1990.
- S. Kohlhoff, P. Gumbsch, and H. F. Fischmeister. Crack propagation in b.c.c. crystals studied with a combined finite-element and atomistic model. *Phil. Mag. A*, 64:851–878, 1991.
- W. Kohn and L. J. Sham. Self-consistent equations including exchange and correlation effects. *Phys. Rev.*, 140(4A):A1133–A1138, 1965.
- E. Kröner. On the physical reality of torque stresses in continuum mechanics. *Int. J. Engng. Sci.*, 1:261–278, 1963.
- L. P. Kubin, G. Canova, M. Condat, B. Devincere, V. Pontikis, and Y. Bréchet. Dislocation microstructures and plastic flow: A 3D simulation. *Solid State Phen.*, 23&24:455–472, 1992.
- B. R. Lawn. *Fracture of Brittle Solids*, Cambridge University Press, Cambridge, UK, 1993.

- A. Leach. *Molecular modelling: principles and applications*. Pearson Education, 2001.
- J. Li. *Handbook of Materials Modeling*, chapter Atomistic Visualization, pages 1051–1068. Springer Netherlands, 2007.
- J. Li, A. H. W. Ngan, and P. Gumbsch. Atomistic modeling of mechanical behavior. *Acta Mater.*, 51:5711–5742, 2003.
- M. Ludwig and P. Gumbsch. An empirical interatomic potential for b2 nial. *Modelling Simul. Mater. Sci. Eng.*, 3:533–542, 1995.
- M. Ludwig and P. Gumbsch. Cleavage fracture and crack tip dislocation emission in B2 NiAl: an atomistic study. *Acta Mater.*, 46:3135–3143, 1998.
- M. Marder and S. Gross. Origin of crack-tip instabilities. *J. Mech. Phys. Solids*, 1:43, 1995.
- J. Marian, W. Cai, and V. V. Bulatov. Dynamic transitions from smooth to rough to twinning in dislocation motion. *Nat. Mater.*, 3:158–163, 2004.
- G. Michot. Fundamentals of silicon fracture. *Crys. Prop. Prep.*, 55:17–18, 1988.
- R. Mikulla, J. Stadler, F. Krul, H.-R. Trebin, and P. Gumbsch. Crack propagation in quasicrystals. *Phys. Rev. Lett.*, 81:3163, 1998.
- R. Miller, M. Ortiz, R. Phillips, V. Shenoy, and E. B. Tadmor. Quasicontinuum models of fracture and plasticity. *Eng. Fract. Mech.*, 61(3-4): 427–444, 1998a. ISSN 0013-7944.
- R. Miller, E. B. Tadmor, R. Phillips, and M. Ortiz. Quasicontinuum simulation of fracture at the atomic scale. *Model. Simul. Mater. Sci. Eng.*, 6(5):607–638, 1998b. ISSN 0965-0393.
- R. E. Miller and E. B. Tadmor. The quasicontinuum method: Overview, applications and current directions. *J. Comput-Aided Mater. Des.*, 9(3): 203–239, 2002. ISSN 0928-1045.
- R. E. Miller and E. B. Tadmor. A unified framework and performance benchmark of fourteen multiscale atomistic/continuum coupling methods. *Model. Simul. Mater. Sci. Eng.*, 17(5):1–51, 2009.
- Y. Mishin, M. J. Mehl, D. A. Papaconstantopoulos, A. F. Voter, and J. D. Kress. Structural stability and lattice defects in copper: ab initio, tight-binding and embedded-atom calculations. *Phys. Rev. B*, 63:224106–1 to 224106–16, 2001.
- M. Mrovec, D. Nguyen-Manh, D. G. Pettifor, and V. Vitek. Bond-order potential for molybdenum: Application to dislocation behavior. *Phys. Rev. B*, 69:094115–1–16, 2004.
- M. Mrovec, R. Gröger, A. G. Bailey, D. Nguyen-Manh, C. Elsässer, and V. Vitek. Bond-order potential for simulations of extended defects in tungsten. *Phys. Rev. B*, 75:104119–1–16, 2007a.

- M. Mrovec, M. Moseler, C. Elsässer, and P. Gumbsch. Atomistic modeling of hydrocarbon systems using analytic bond-order potentials. *Prog. Mater. Sci.*, 52:230–254, 2007b.
- J. Nocedal and S. J. Wright. *Numerical Optimization*. Springer, New York, 2006.
- M. Ortiz and R. Phillips. Nanomechanics of defects in solids. In *Adv. Appl. Mech.*, volume 36, pages 1–79. Academic Press, 1999.
- K. C. Pandey. New π -bonded chain model for si (111)-(2 \times 1) surface. *Phys. Rev. Lett.*, 47:1913, 1981.
- M. Parinello and A. Rahman. Crystal structure and pair potentials: a molecular dynamics study. *Phys. Rev. Lett.*, 45:1196–1199, 1980.
- L. Pastewka, P. Pou, R. Pérez, P. Gumbsch, and M. Moseler. Describing bond-breaking processes by reactive potentials: Importance of an environment-dependent interaction range. *Phys. Rev. B*, 78:161402, 2008.
- R. Pérez and P. Gumbsch. An ab initio study of the cleavage anisotropy in silicon. *Acta Mater.*, 48:4517, 2000a.
- R. Pérez and P. Gumbsch. Directional anisotropy in the cleavage fracture of silicon. *Phys. Rev. Lett.*, 84:5347, 2000b.
- D. G. Pettifor. *Bonding and Structure of Molecules and Solides*. Oxford University Press, 1995.
- D. G. Pettifor and I. I. Oleinik. Analytic bond-order potentials beyond Tersoff-Brenner. I. Theory. *Phys. Rev. B*, 59:8487–8499, 1999.
- T. Pöschel and T. Schwager. *Computational Granular Dynamics*. Springer, 2005.
- D. C. Rapaport. *The Art of Molecular Dynamics Simulation*. Cambridge University Press, 2004.
- J. Riedle, P. Gumbsch, and H. F. Fischmeister. Cleavage anisotropy in tungsten single crystals. *Phys. Rev. Lett.*, 76:3594–3597, 1996.
- R. E. Rudd and J. Q. Broughton. Coarse-grained molecular dynamics and the atomic limit of finite elements. *Phys. Rev. B*, 58(10):R5893–R5896, 1998. ISSN 0163-1829.
- R. E. Rudd and J. Q. Broughton. Concurrent coupling of length scales in solid state systems. *Phys. Status Solidi B-Basic Solid State Phys.*, 217(1):251–291, 2000. ISSN 0370-1972.
- R. E. Rudd and J. Q. Broughton. Coarse-grained molecular dynamics: Nonlinear finite elements and finite temperature. *Phys. Rev. B*, 72(14), 2005. ISSN 1098-0121.
- C. Rudhart, P. Gumbsch, and H.-R. Trebin. *Quasicrystals, Structure and Physical Properties*, H.-R. Trebin (ed.), Wiley-VCH, Weinheim, page 484, 2003.

- T. Schlick. *Molecular Modeling and Simulation: An Interdisciplinary Guide*. Springer, 2002.
- R. L. B. Selinger and D. Farkas. Atomistic theory and simulation of fracture. *MRS Bull.*, 25/5:11, 2000.
- V. B. Shenoy, R. Miller, E. B. Tadmor, D. Rodney, R. Phillips, and M. Ortiz. An adaptive finite element approach to atomic-scale mechanics - the quasicontinuum method. *J. Mech. Phys. Solids*, 47(3):611–642, 1999. ISSN 0022-5096.
- J. R. Shewchuk. An introduction to the conjugate gradient method without the agonizing pain, 1994. URL <http://www.cs.cmu.edu/~jrs/jrspapers.html#cg>.
- L. E. Shilkrot, W. A. Curtin, and R. E. Miller. A coupled atomistic/continuum model of defects in solids. *J. Mech. Phys. Solids*, 50(10):2085–2106, 2002. ISSN 0022-5096.
- L. E. Shilkrot, R. E. Miller, and W. A. Curtin. Multiscale plasticity modeling: coupled atomistics and discrete dislocation mechanics. *J. Mech. Phys. Solids*, 52(4):755–787, 2004. ISSN 0022-5096.
- T. Shimokawa, J. J. Mortensen, J. Schiotz, and K. W. Jacobsen. Matching conditions in the quasicontinuum method: Removal of the error introduced at the interface between the coarse-grained and fully atomistic region. *Phys. Rev. B*, 69(21):214104, 2004. ISSN 1098-0121.
- G. C. Sih and H. Liebowitz. Mathematical theories of brittle fracture. In H. Liebowitz, editor, *Fracture*, volume 2, pages 67–190, New York, 1968. Academic Press.
- R. Sunyk and P. Steinmann. On higher gradients in continuum-atomistic modelling. *Int. J. Solids Struct.*, 40(24):6877–6896, 2003. ISSN 0020-7683.
- J. G. Swadener, M. I. Baskes, and M. Nastasi. Molecular dynamics simulation of brittle fracture in silicon. *Phys. Rev. Lett.*, 89:085503, 2002.
- E. B. Tadmor, M. Ortiz, and R. Phillips. Quasicontinuum analysis of defects in solids. *Phil. Mag. A*, 73(6):1529–1563, 1996. ISSN 0141-8610.
- P. W. Tasker. Surfaces and interfaces in ionic materials. In G. Jacucci, editor, *Computer Simulation in Physical Metallurgy*, pages 21–40. ECSC, EEC, EAEC, Brussels and Luxembourg, 1986.
- R. Thomson, C. Hsieh, and J. Rana, V. Lattice trapping of fracture cracks. *Appl. Phys.*, 42:3154., 1971.
- G. J. Wagner and W. K. Liu. Coupling of atomistic and continuum simulations using a bridging scale decomposition. *J. Comput. Phys.*, 190(1): 249–274, 2003. ISSN 0021-9991.
- D. Weygand and P. Gumbsch. Study of dislocation reactions and rearrangements under different loading conditions. *Mat. Sci. Eng. A*, 400:158–161, 2005.

- D. Weygand, L. H. Freidman, E. Van der Giessen, and A Needleman. Aspects of boundary-value problem solutions with three-dimensional dislocation dynamics. *Model. Simul. Mater. Sci. Eng.*, 10:437–468, 2002.
- G. Zanzotto. The Cauchy-Born hypothesis, nonlinear elasticity and mechanical twinning in crystals. *Acta Crystallogr. Sect. A*, 52(Part 6):839–849, 1996. ISSN 0108-7673.
- S. J. Zhou, D. M. Beazley, P. S. Lomdahl, and B. L. Holian. Dynamic crack processes via molecular dynamics. *Phys. Rev. Lett.*, 76:2318–2321, 1996.
- J. A. Zimmerman, C. L. Kelchner, P. A. Klein, J. C. Hamilton, and S. M. Foiles. Surface step effects on nanoindentation. *Phys. Rev. Lett.*, 86:165507–1 to 165507–4, 2001.

